Universidade de Aveiro
Ano 2012

Departamento de Fisica

BAIBA NIPARTE

ESTUDOS DE SUPER-HIDROFILICIDADE EM FILMES NANOCOMPOSITOS DE TiO_2-SiO_2

NEW INSIGHTS IN SUPER-HYDROPHILICITY OF TiO_2-SiO_2 NANOCOMPOSITE FILMS

Universidade de Aveiro
Ano 2012

Departamento de Fisica

BAIBA NIPARTE

ESTUDOS DE SUPER-HIDROFILICIDADE EM FILMES NANOCOMPOSITOS DE TiO_2-SiO_2

NEW INSIGHTS IN SUPER-HYDROPHILICITY OF TiO_2-SiO_2 NANOCOMPOSITE FILMS

Dissertação apresentada à Universidade de Aveiro para cumprimento dos requisitos necessários à obtenção do grau de **Mestre em Mestrado em Ciência e Engenharia de Materiais (Functionalized Advanced Materials and Engineering (FAME))**, realizada sob a orientação científica Investigador Coordenador **MICHEL LANGLET** de CNRS – LMGP (França), e Professor **TITO DA SILVA TRINDADE** do Departamento de Quimica da Universidade de Aveiro

o júri

Presidente	Prof. Doutora Ana Margarida Madeira Viegas de Barros Timmons Professora Auxiliar, Universidade de Aveiro
Arguente Principal	Prof. Doutora Paula Alexandrina de Aguiar Pereira Marques Equiparada a Investigadora Auxiliar, Universidade de Aveiro
Orientador	Prof. Doutor Michael Langlet Investigador Coordenador, CNRS – França
Co-Orientador	Prof. Doutor Tito da Silva Trindade Professor Associado Com Agregação, Universidade de Aveiro

palavras-chave

Hidrofilicidade, compósitos de TiO_2-SiO_2, porosidade artificial, esferas de poliestireno, processo sol-gel, método *spin-coating*

resumo

Os efeitos resultantes da hidrofilicidade de compósitos TiO_2-SiO_2 com diferente reatividade e composição química em processos sol-gel têm sido descritos na literatura. Esses resultados mostram que formulações sol-gel menos reativas originam super-hidrofilicidade, isto é, um ângulo de contacto inferior a 10° após envelhecimento superior a 8 semanas (envelhecimento em condições ambiente). Tendo em conta a morfologia de derivados de filmes compósitos e diferentes modelos termodinâmicos de superficie, sugere-se que um filme compósito com uma textura mais porosa poderá levar a um efeito de super-hidrofilicidade superior. Para verificar esta hipótese, neste projeto optou-se por estudar em detalhe compósitos TiO_2-SiO_2 mais reativos com diferentes composições (0, 20, 60 e 100 mol% de SiO_2), em que a uma maior reatividade sol-gel é esperada uma redução da super-hidrofilicidade dos filmes compósitos. Com o objetivo de criar artificialmente uma morfologia rugosa/porosa, utilizaram-se neste caso camadas de esferas de poliestireno (PS) com um diâmetro médio de 0.6 μm.

Com o objetivo de definir as melhores condições para obter camadas compactas 2D de esferas de PS foram estudados diferentes parâmetros no método de revestimento *spin-coating*. Realizaram-se experiências com diferentes velocidades de rotação (1000rpm e 500rpm). Outros parâmetros de deposição por *spin-coating* ajustados foram a rotação a 5000rpm/s, tempo de rotação de 1s, concentração de esferas de PS a 1wt% em EtOH, e um volume de 100μL para a solução de PS. As camadas 2D de PS foram posteriormente impregnadas em sóis de TiO_2-SiO_2. A utilização de esferas de PS permitiu obter filmes compósitos de TiO_2-SiO_2 com rugosidade aproximadamente cem vezes superior aos filmes compósitos obtidos na ausência das esferas de PS. Estas características morfológicas foram confirmadas por microscopia ótica, microcopia eletrónica (SEM) e microscopia de força atómica (AFM). Por sua vez, medições do ângulo de contacto mostraram que a hidrofilicidade aumenta após as modificações morfológicas efetuadas e, nos melhores casos (amostras com 20-60 mol% de SiO_2), os ângulos de contacto de água obtidos foram inferiores a 5^o, após 6 semanas de envelhecimento (sob condições ambiente). Este estudo mostrou igualmente que nestes casos existe uma relação entre: 1) o revestimento da superfície das esferas de PS, 2) a rugosidade/porosidade da superfície dos filmes S1-X+PS, e 3) a persistência da super-hidrofilicidade.

keywords

Hydrophilicity, TiO_2-SiO_2 composites, artificial porosity, polystyrene beads, sol-gel process, spin-coating method

abstract

Enhanced hydrophilicity effects arising from TiO_2-SiO_2 granular interfaces in composite films deposited via sol-gel routes have been studied before. Results obtained so far have shown that sol-gel formulations yielding less reactive sols lead to enhanced super-hydrophilicity persistence of composite films, i.e. a water contact angle less than 10^o after aging for more than 8 weeks (aging under ambient conditions without UV radiation). Taking into account the morphology of derived composite films and different surface thermodynamics models, we have suggested that a more rough/porous structure of the composite film might even increase this enhanced hydrophilicity effect. To verify this hypothesis, we have chosen to study more reactive TiO_2-SiO_2 composite sols with different compositions (0, 20, 60 and 100mol% of SiO_2). This greater sol-gel reactivity is expected to reduce the natural super-hydrophilicity of composite films in order to better assess eventual effects of the morphology. Then, in order to artificially create rough/porous morphologies, we have used polystyrene (PS) beads with average diameter of *0.6µm*.

Different parameters of spin-coating deposition method were tested to define the best conditions to obtain 2D layers of closely packed PS beads. Further, two experiments with different rotation speeds (1000rpm and 500rpm) were performed. Other spin-coating conditions were fixed as follows: acceleration of 5000rpm/s, rotation time of 1s, concentration of PS beads 1wt% in EtOH, volume of PS solution 100µL. Such 2D PS layers were then impregnated with TiO_2-SiO_2 composite sols. Using PS beads, we have obtained TiO_2-SiO_2 composite films with a roughness that is almost 100 times higher than composite films without PS beads. These morphology features are confirmed by optical microscopy, AFM and FEG-SEM measurements. Water contact angle measurements show in turn that the hydrophilicity effects are increased by morphologic modifications, and in the best cases (samples with 20-60mol% of SiO_2) water contact angles are close to 5^o after 6 weeks of aging under ambient conditions without UV radiation. This study also shows that, in these cases, there is some relation between: 1) the surface coverage of PS beads, 2) the surface roughness/porosity of S1-X+PS films, and 3) their super-hydrophilicity persistence.

List of Figures and Tables

Contents

1. Introduction

The concept of "self-cleaning surfaces" has been a subject of particular interest for the past decades and the research field in this direction has increased significantly. Photo-induced properties of titanium dioxide (TiO_2) coatings, when exposed to UV radiation, allow development of the studies. However, Manuel Houmard in his PhD thesis work in *Laboratoire des Matériaux et de Génie Physique (LMGP)* of Grenoble INP has shown that, contrary to TiO_2 coatings that need to be exposed to UV radiation, TiO_2-SiO_2 nano-composite coatings obtained by sol-gel method show a natural super-hydrophilicity of the surface. This property allows natural and efficient elimination of pollution (oils or others) present on the surface just by simple washing with water without need of different detergents or exposure to UV radiation.

Although the "self-cleaning" functionality of TiO_2-SiO_2 nano-composite coatings obtained by sol-gel method has already been shown and proven at LMGP, the origin of this super-hydrophilicity effect still raises questions, particularly about the nature of the nano-composite. Answers to these questions would make not only a progress in knowledge about the fundamental mechanisms responsible about this property, but also provide possibilities for further optimization of the functionality. This Master thesis work is a part of that goal.

2. Theoretical description and generalities

2.1. Super-hydrophilicity: photo-induced property

In order to consider a material as hydrophilic, it should exhibit a strong surface energy and have the possibility to create hydrogen bonds with water. This hydrophilic property is described by a water contact angle value that is lower than 90^o in contact with the surface of the material. First researches on photo-induced properties of titanium dioxide (TiO_2) date from 1970, when the work of Fujishima et al. showed that a TiO_2 electrode, when irradiated with UV, could decompose the water into hydrogen and oxygen [1]. Such photo-induced reaction results from the fact that TiO_2 is a semiconductor with different energies for the valance band (VB) and conduction band (CB), creating an energy gap between both levels. Thus, when TiO_2 absorbs a photon with energy that is higher or equal to that of the band gap, an electron-hole pair is generated, where the electron (hole) is excited from the VB (CB) to the CB (VB) [2]. The charge carriers are therefore generated in the form of photo-electrons (e^-) and photo-holes (h^+) by the following reaction:

$$TiO_2 + h\nu \rightarrow e^- + h^+ \quad (1)$$

These photo-generated charges are responsible for the high photo-catalytic activity of TiO_2 because the formation of highly reactive species, such as hydroxyl radicals (OH•), leads to the degradation of the pollution adsorbed on the surface via red-ox reactions.

Another interesting property of TiO_2 is its photo-induced super-hydrophilicity. Wong et al. have shown that the increased super-hydrophilicity of TiO_2 is not uniform but involves localized domains that are favorable to the water adsorption [3,4]. Photo-generated electrons tend to reduce the cations Ti^{4+} in Ti^{3+} (equation (2)), meanwhile the holes are trapped in the oxygen network within the TiO_2 matrix (equation (3)). This insertion of holes weakens the linking between the oxygen atoms and associated titanium atoms, thus favoring the formation of oxygen vacancies on the surface of TiO_2 (equation (4)) [5,6]:

$$e^- + Ti^{4+} \rightarrow Ti^{3+} \text{ (electron trapping)} \quad (2)$$

$$h^+ + O^{2-} \rightarrow O^- \text{ (hole trapping)} \quad (3)$$

$$h^+ + O^- \rightarrow \tfrac{1}{2}\, O_2 + O\bullet \text{ (formation of oxygen vacancy)} \quad (4)$$

The oxygen vacancies are then able to promote a molecular or dissociative adsorption of the atmospheric water, producing surface OH groups. Thus, the functionalized surface has a great affinity for the water that gives its super-hydrophilic properties, determined by a water contact angle close to zero (see Fig. 1). It has also been shown that other parameters such as roughness and ambient atmosphere might influence the photo-induced super-hydrophilicity of the material [7,8].

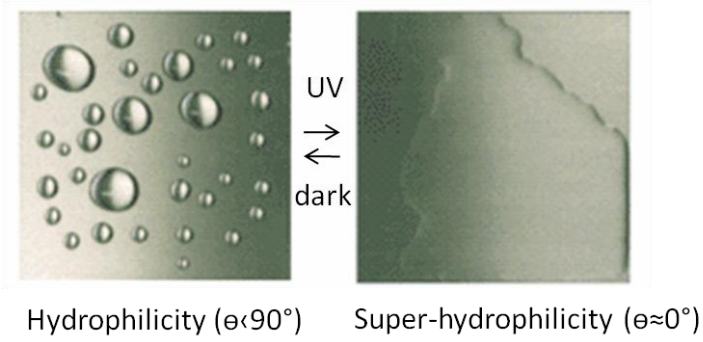

Fig. 1: Illustration of the photo-induced super-hydrophilicity of a TiO_2 coating [6]

These photo-induced properties are the objects of mainly extensive studies for self-cleaning applications in outdoor atmosphere, i.e. atmosphere which takes advantage of solar UV light and rain water to remove carbon pollution.

2.2. New alternatives

Previous studies have shown that the addition of SiO_2 into the TiO_2 film decreases the water contact angle and this effect might last for several days [9]. In his PhD thesis held in *LMGP*, M. Houmard has improved this tendency by studying sol-gel thin films of TiO_2-SiO_2 nano-composites [10]. These layers show a natural super-hydrophilicity and this property can persist for several weeks or months in the absence of UV light. This natural super-hydrophilicity allows new developments of "self-cleaning" surfaces entirely based on natural super-hydrophilic properties in atmosphere where UV light cannot be present permanently or in strong dose, i.e. indoor atmosphere.

2.3. Mechanisms of super-hydrophilicity of TiO_2-SiO_2 nano-composites with granular interfaces

By following the evolving kinetics of water contact angle on the film surface over aging without UV radiation, M. Houmard has shown the beneficial effect of TiO_2-SiO_2 granular

interfaces on the natural super-hydrophilicity of derived composite films. As seen in Fig. 2, the reference films of pure TiO_2 and pure SiO_2 have a super-hydrophilic effect only for the first few hours or days, which disappears rapidly without UV radiation. Meanwhile, the composite conserves its super-hydrophilicity for a very long time, i.e. a water contact angle smaller than 5^o after eight weeks of aging [10].

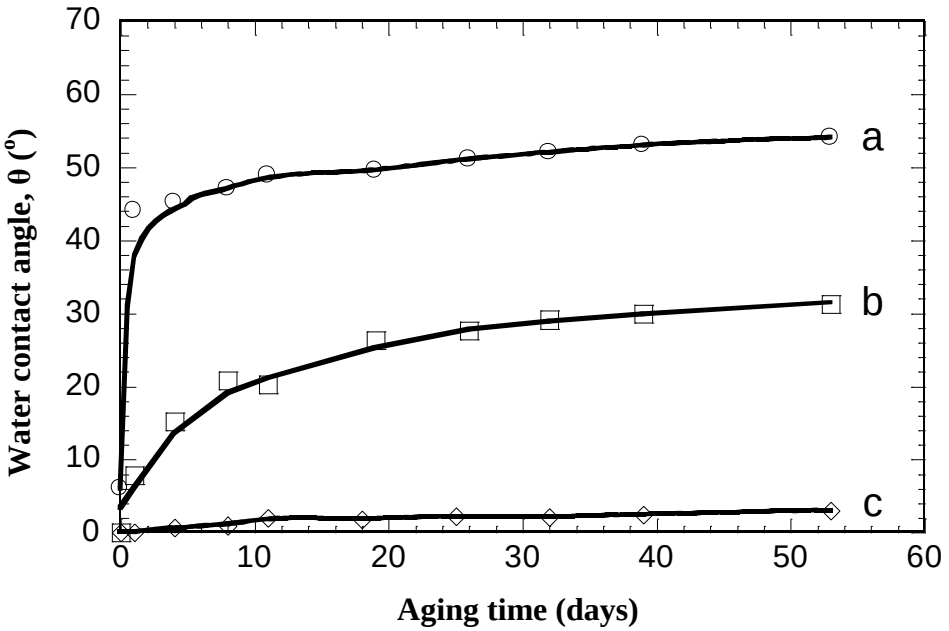

Fig. 2: Kinetics of evolution of the water contact angle on three different surfaces as a function of aging in the ambient atmosphere and without UV irradiation: (a) pure TiO_2, (b) pure SiO_2 and (c) a TiO_2-SiO_2 composite film deposited from a sol with SiO_2 concentration of 60mol% [10]

Although, the morphology of composite films is a factor that might influence their super-hydrophilicity, another hypothesis would be the formation of deprotonated TiO_x^- and/or protonated SiO_x^+ units at the TiO_2-SiO_2 granular interfaces of composite films. These interfacial charges have been frequently mentioned as the main reason for the catalytic behavior of TiO_2-SiO_2 composites [10]. In our case, charges that appear on the surface of composite films can induce the molecular or dissociative adsorption of the atmospheric water resulting in the super-hydrophilicity. Thus, the water contact angle for the TiO_2-SiO_2 composite material is never between those of pure TiO_2 and pure SiO_2 as one would expect. Fig. 3 represents the water contact angle measured after eight weeks of aging under ambient atmosphere without UV irradiation as a function of the sol TiO_2-SiO_2 molar

composition. These results show that the best persistence of the super-hydrophilicity is observed for those composites that have more TiO_2-SiO_2 interfaces with an optimum composition containing 40-60mol% of SiO_2. This observation reinforces the assumption that the natural super-hydrophilicity arises, at least partially, from interfaces effects. As will be detailed in next section the sol-gel reactivity is another factor that can influence interfaces effects.

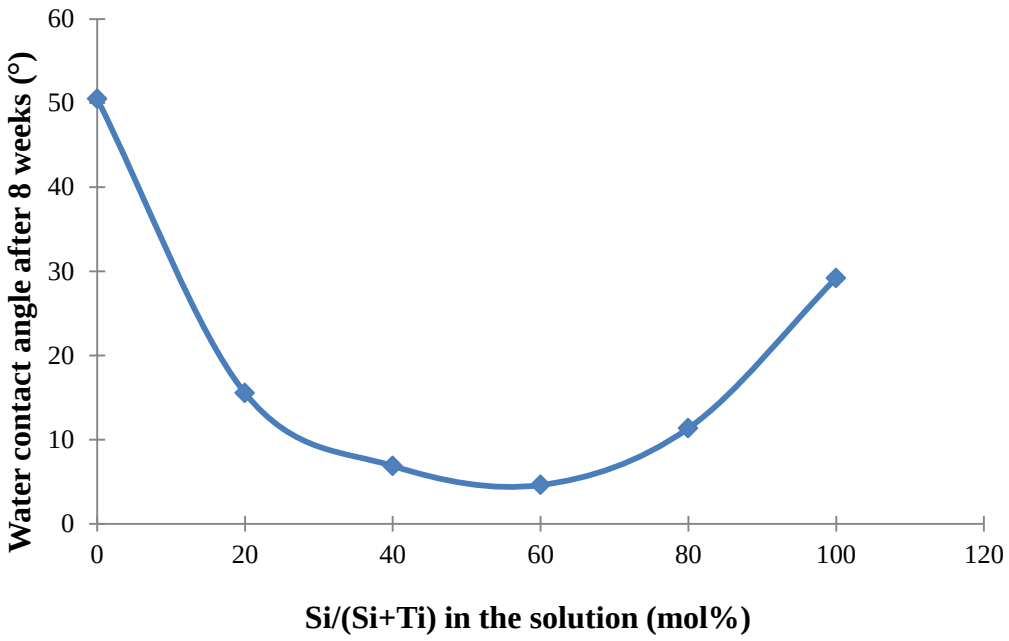

Fig. 3: Water contact angle measured after eight weeks of aging under ambient atmosphere without UV irradiation as a function of the SiO_2 sol molar composition [10]

As it was mentioned before, morphology of the composite films can also strongly influence their natural super-hydrophilic behavior. Indeed, it is known that a naturally hydrophilic surface becomes even more hydrophilic when being porous or rough (see section 3.5.1). Previous studies have revealed the porosity and roughness of TiO_2-SiO_2 composite films, where composite films with best super-hydrophilicity persistence have an RMS roughness of about 10 nm, compared to 5 nm and less than 1 nm for pure TiO_2 and SiO_2 films, respectively. The optimized composite films also exhibit a porous sponge-like morphology that is characterized by big surface cavities (see dark areas in FEG-SEM and AFM images of Fig. 4). Thus, it remains important to assess how the effects of granular interfaces and morphology respectively influence the natural super-hydrophilicity of TiO_2-SiO_2 composites. This Master thesis work is a contribution to this objective.

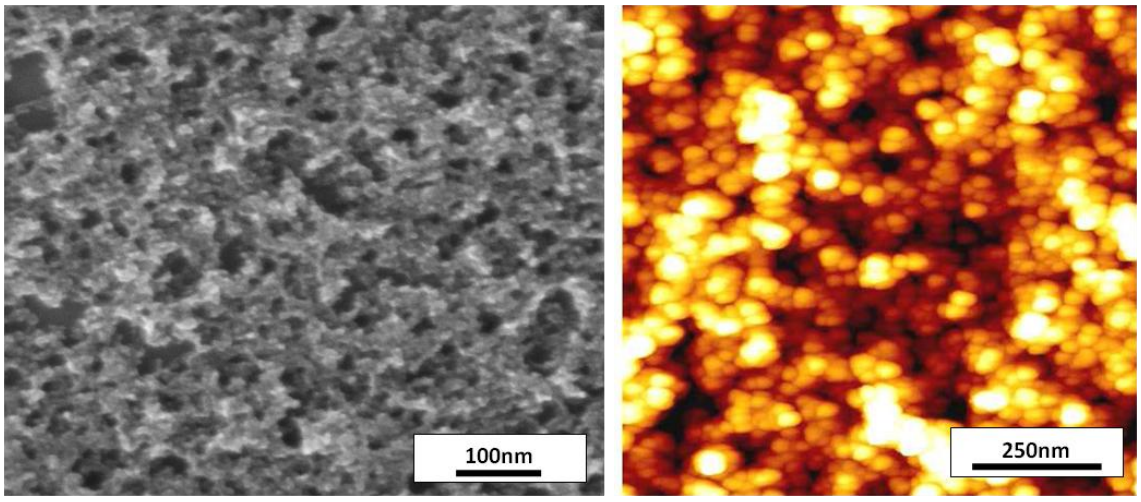

Fig. 4: FEG-SEM (left) and AFM (right) images of the optimized composite film [10]

2.4. Cleanability

In last decades, many studies have been devoted to the detachment of an oil drop deposited on a surface by using skimming flow [11,12]. Inspired by these works, *SIMaP* laboratory of Grenoble INP has developed an experimental setup for dynamic wetting tests, which uses skimming flow of water to simulate the cleaning of a surface previously polluted with oil [13,14]. This device implements a cell with laminar flow that is associated with an optical device that follows the evolution of the oil drop in real time when increasing the water flow. The minimal critical flow that is needed to completely detach the oil drop provides quantitative information on the water cleanability of the surface.

These flow measurements were performed to detach an oil drop from the surfaces of various TiO_2-SiO_2 compositions aged under ambient atmosphere during 8 weeks without UV light. Results illustrated in Fig. 5 demonstrate a perfect correlation between enhanced super-hydrophilicity persistence, as shown in Fig. 3, and a reduced critical flow of water, proving that the cleanability of the composite surfaces directly arises from their super-hydrophilicity.

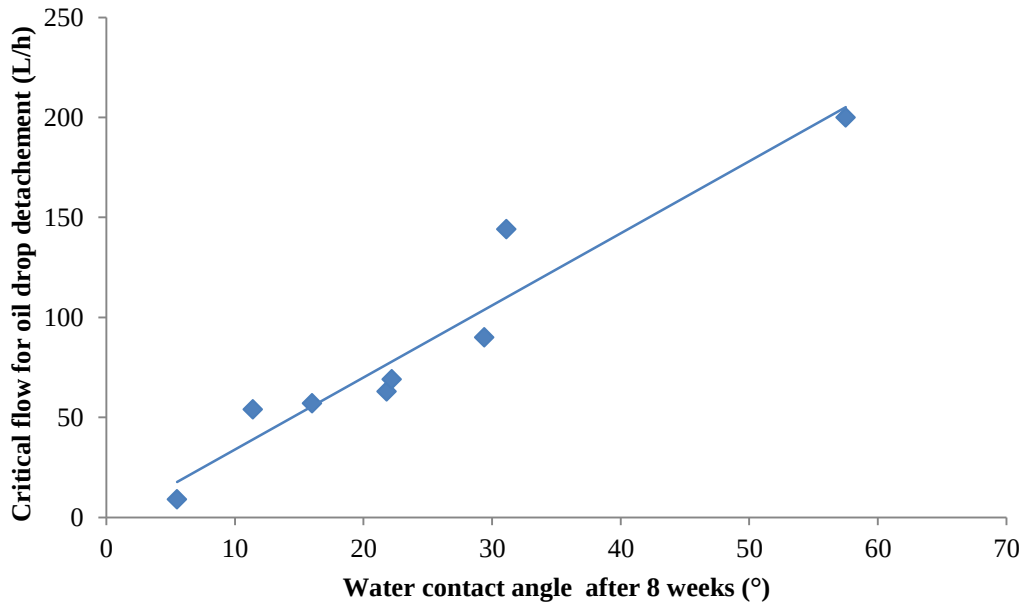

Fig. 5: Critical flow to detach oil drop as a function of water contact angle measured on various composite coatings after 8 weeks of aging [10]

2.5. Artificial porosity/roughness

Since an enhanced roughness or surface porosity of TiO_2-SiO_2 composite films can favor their natural super-hydrophilicity, the aim of this Master thesis work has been to artificially increase the porous/rough structure of TiO_2-SiO_2 composites in order to assess how this modification influences the water wettability. It is known that the use of differently sized porogenes (macro- and meso-sized) results in aligned and closely packed pores leading to structures of controlled porosity, pore size, and surface area [15]. For instance, previous studies have shown that one can obtain architectured macro-meso-microporous structures with 3D interconnectivity by using polystyrene (PS) latex spheres, copolymers such as Pluronic F127 or P123, and alcohol as co-surfactant (see Fig. 6) [16].

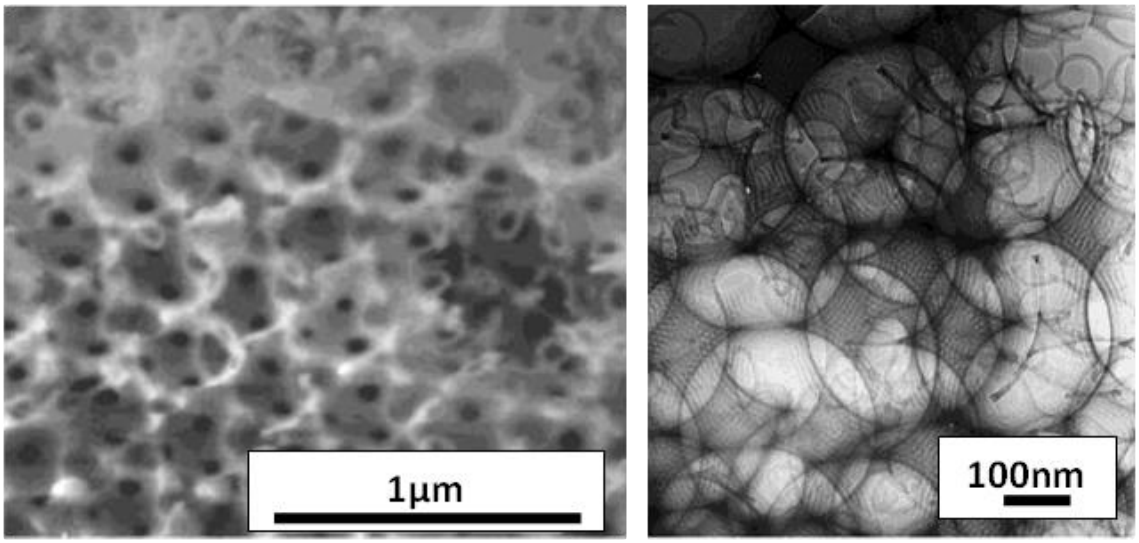

Fig. 6: SEM micrograph (left) and TEM image (right) of macro-meso-microporous structure of SiO_2 obtained with template of polystyrene latex spheres with average diameter size of 485nm, Pluronic F127 as surfactant, *n*-pentanol as co-surfactant; reprinted from [16]

In this work, we have used such results to artificially form macro-porous structures (a typical pore dimension of some hundreds of nanometers) from PS beads. According to the literature and as illustrated in Fig. 7, this approach relies on the preliminary formation of a composite monolith constituted of PS beads and an inorganic network, for instance SiO_2 in the example illustrated in Fig. 6. PS beads are subsequently eliminated through solvent extraction or calcination, which yields a residual inorganic rough and porous network.

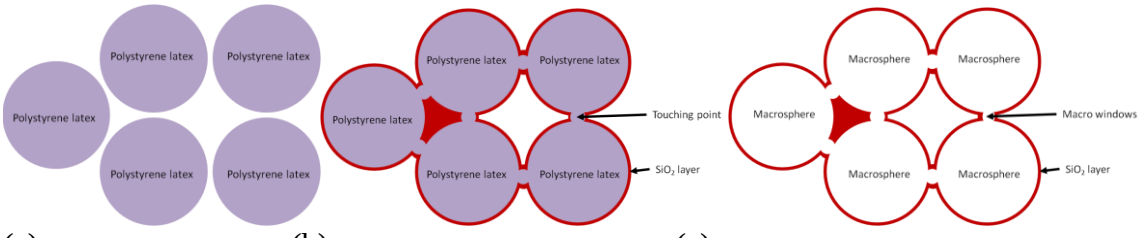

Fig. 7: Schematic representation of the macro-pores formation: (a) composite monolith constituted of PS beads, (b) when inorganic SiO_2 solution diffuses into the interstitial voids of PS monolith, it precipitates around the PS beads, and (c) removing the PS beads yields a macro-porous inorganic network, adapted from [16]

In the recent literature, the artificial formation of porous inorganic networks has generally been devoted to 3D structures [15,16]. In contrast, we have chosen to focus the present work on the 2D assembly (single-layer) of closely-packed PS nano-beads that would be

used as a template to create a rough and macro-porous structure from TiO_2-SiO_2 composites. In order to reach this goal, one has first to study the elaboration of closely-packed PS single-layers by a spin-coating technique, which can subsequently be impregnated with a composite sol.

2.6. 2D assembly of PS beads by spin-coating method

2.6.1. 2D assembly of PS beads

The very first descriptions about the basic formation mechanisms of 2D ordered clusters from colloidal particles on a substrate were proposed in 1909 by J. Perrin [17]. Based on this work, Denkov et al. more recently re-described the 2D ordering of micrometer-size polystyrene latex spheres on a horizontal glass substrate by means of optical microscopy observations [18]. They have proven that the main factors governing the ordering are: 1) the attractive capillary forces caused by the liquid (generally water) menisci formed around the particles and 2) the convective transport in liquid medium of particles toward the ordered region (see Fig. 8a). Further, the formation of well-ordered single-layers or well-ordered domains consisting of multilayers (bi-layers, tri-layers, etc.) can be controlled by the water evaporation rate (see Fig. 8b).

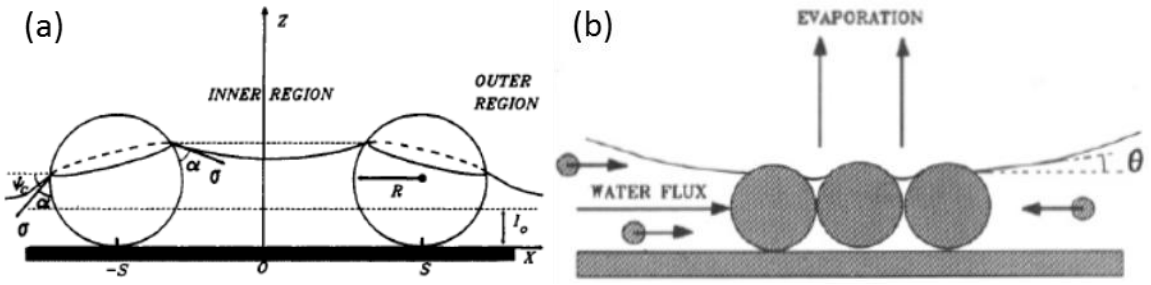

Fig. 8: Schematic representation of (a) two PS spheres partially immersed in a liquid layer on a horizontal solid substrate showing that the deformation of the liquid meniscus gives rise to inter-particle attraction; and (b) convective flux toward the ordered phase due to the water evaporation from the menisci between the particles in the 2D array; reprinted from [18]

At the first stage, a "nucleus" of ordered phase appears when the upper surface of the thinning aqueous layer in the wetting film presses the latex particles toward the water-glass interface. The ordering of PS spheres starts when the thickness of the water layer containing PS particles becomes approximately equal to the diameter of particles. From

here, one can define the second stage of the 2D crystal growth when the horizontal component of capillary forces (i.e. convective water flux) causes the directional motion of particles toward the ordered array and the evaporation of water leads to a gradual decrease of the liquid layer thickness with time. That increases the curvature and hence the local sucking capillary pressure causing an intensive water influx from the thicker parts of the liquid layer where the pressure is higher [18].

The described mechanisms suggest at least two ways to control the ordering process: 1) control of the speed of the convective flow by changing the rate of water evaporation and 2) control of the profile of the liquid meniscus encircling the ordered array by ejecting (injecting) some amount of suspension during the experiment. In both cases the mechanisms lead to a change of the liquid layer thickness and a surface slope at the boundary between the array and the encircling meniscus. Nevertheless, large mono-crystal domains (better quality of 2D arrays) can be obtained when the rate of 2D crystal growth is lower [18].

2.6.2. Spin-coating method

In this work, we have studied the liquid deposition of 2D PS structures using a spin-coating method (see Fig. 9). The general description of this method relies on four steps: 1) deposition of the material where the deposited liquid solution wets the substrate; 2) radial acceleration where the centrifugal force generated by the rotation of the substrate pushes the liquid towards the edges of the substrate and covers it fully; 3) constant rotation where the liquid film homogenizes and the extra amount of liquid is ejected from the substrate due to the centrifugal force; and 4) solidification where the evaporation of the solvent (which might occur already during the steps 2 and 3) yields a film constituted of solid particles initially diluted in the liquid or activates organic or inorganic (sol-gel, see after) polymerization reactions leading to solid thin film formation [10].

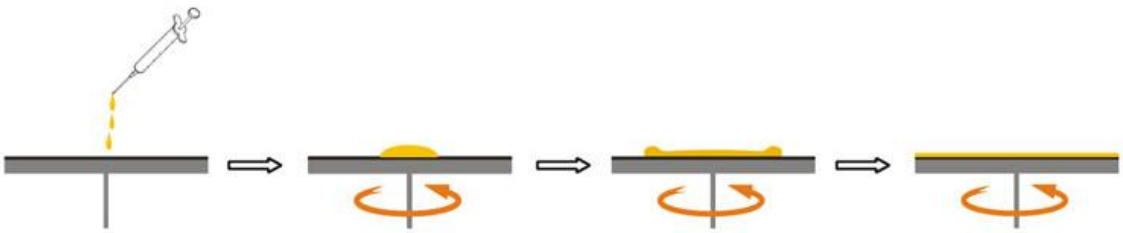

Fig. 9: Schematic representation of spin-coating method

One has to take into account that the layer formation from colloidal solution with polymer beads (or other kinds of solid particles diluted in a liquid) by spin-coating method is not the same as in the case of polymeric solutions. Thus, in our case, the basic mechanisms of thin film formation from polymeric solutions cannot be applied completely. Actually, only few research papers have described the use of spin-coating technique in order to obtain 2D assembly of PS nano-spheres [19-21]. According to these papers, in the case of colloidal suspensions, there are two types of parameters that have to be considered and to be adjusted during deposition process. One has to estimate, a) the parameters of the colloidal suspension: such as the diameter of PS beads, concentration, surfactants on the surface of nano-spheres, solvents etc., and b) the parameters for the spin-coating method: rotation speed, rotation duration, acceleration, deposited volume of suspension etc. This huge range of experimental parameters does not allow to a-priori fix one possible approach to obtain best 2D PS assemblies. For instance, some recent papers have shown that variation of the parameters involved in the spin-coating deposition of PS micro-beads yield a wide range of results in terms of 2D-assembly performances [20,21]. Thus, a first goal of this work has been to find the assembly conditions in relation to our final objective. Let us recall that the 2D PS assembly intended here corresponds to a preliminary step, which will be followed by the impregnation of composite sols in order to finally create an artificially enhanced roughness or porosity of TiO_2-SiO_2 composite films. For this subsequent composite sols impregnation, we have directly extrapolated spin-coating deposition conditions habitually used for the formation of composite films. These conditions will be recalled in following sections. In this work, silica wafers were used as substrates.

3. Characterization methods

All the physicochemical and morphological characterization methods described in this work have been done in *LMGP* and *SIMaP* laboratories of Grenoble INP.

3.1. Optical Microscopy (OM)

Optical microscopy, employed to obtain an enlarged image of a small object, uses visible light and modifies the path of the light to generate an improved contrast image from a sample. For analysis of surface structures, one can use transmitted or reflected light configurations. In our case, as the substrate used for the sample preparation is Si (non-transparent), the sample illumination is done from the top of the sample (reflected light detection). Observations with optical microscope allow obtaining a general description of the sample surface to anticipate further experiments.

3.2. Coverage Rate (CR)

Surface coverage rate quantitatively describes the rate of the polystyrene beads covering the substrate and permits quantitative analysis of obtained samples. In order to calculate CR, a program called *'ImageJ'* is used. This program uses optical images and, applying a threshold function, compares 'white areas' with 'black areas' observed in the pictures.

3.3. Scanning Electron Microscopy (SEM)

Scanning electron microscopy technique is based on the principle of the electron-medium interactions. Electron beam scans the surface of the sample reemitting different radiation (secondary electrons, backscattered electrons, Auger electrons, X-rays). Different detectors allow analyzing the reemitted radiations, reconstruct the image of the surface and determine chemical elements present in the zone of analysis. Morphological and micro-structural characterization of TiO_2-SiO_2 composite thin films was done using a pressure controlled FEG (Field Emission Gun) SEM microscope.

3.4. Atomic Force Microscopy (AFM)

Atomic force microscopy (AFM) permits to study the sample surface topography. The principle of this technique is based on the interactions between the sample and a tip attached on a micro-lever. The tip scans the surface of the sample and, according to feedback parameters, changes its height. Computer registers the height and reconstructs an

image of the surface. Roughness of the surface is characterized by the RMS (Root Mean Square) value. AFM measurements are recorded in 'tapping' mode using a silicon nitride tip with a curvature radius of around 15nm.

3.5. Wetting – water contact angle measurements

3.5.1. Theory

The wettability measurements are widely employed techniques in studies of surface properties and are usually used to characterize the affinity between a solid and a liquid by measuring the liquid contact angle θ formed between the liquid and solid surface as shown in Fig. 10.

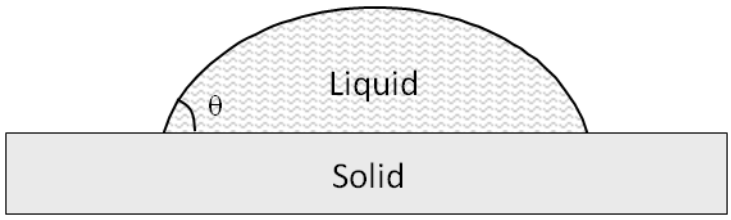

Fig. 10: Schematics of contact angle θ formed between a liquid drop and a solid surface

In this work, the water contact angles were measured using the sessile drop method. When the drop is deposited on the solid surface, it acquires particular configuration that describes interactions occurring at the solid/liquid interface (see Fig. 11).

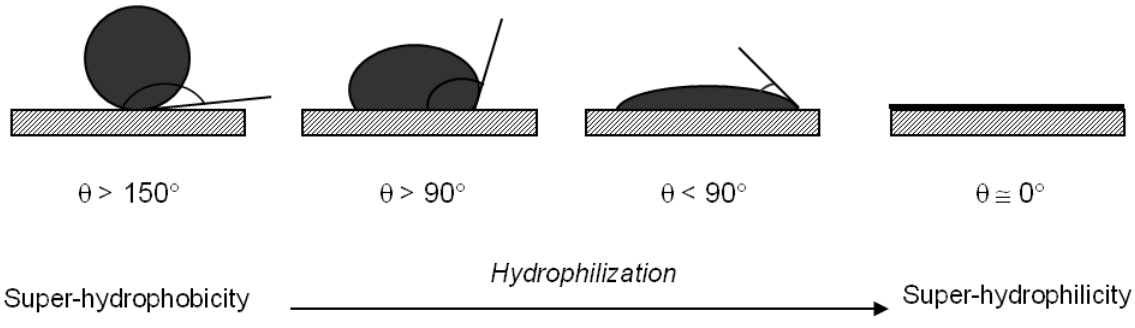

Fig. 11: Schematics of water contact angle θ formed between liquid drop and solid surface as a function of its hydrophobic/hydrophilic characteristics

As it was described in paragraph 2, creation of a rough surface is the aim of this thesis work. Therefore, one has to take into account the effects that occur on a rough surface when a water droplet touches it. M. Houmard in his PhD Thesis work [10] has described

three possible models related to so-called textured surface: 1) Cassie-Baxter's model [22] that describes a chemically heterogeneous surface, 2) Wenzel's model [23] describing a rough surface and 3) Bico's model [24] that relates both previous models describing a structure with an open surface porosity. All three models, in general, are described similarly, taking into account interacting surfaces (liquid-liquid, liquid-solid). For instance, in the Bico's model, the porous (rough) surface is described as a composite one, one component being the dry solid itself, the other one being constituted of impregnated water regions (see Fig. 12).

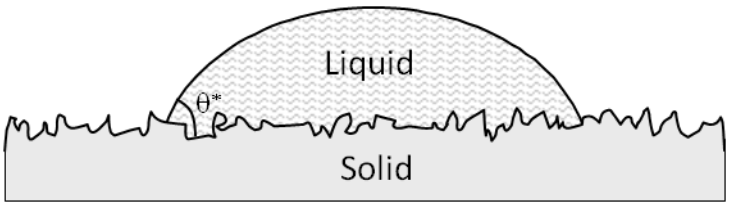

Fig. 12: Schematics of water contact angle formed between a liquid drop and a surface with an open porosity

In this case the measured water contact angle θ^* is defined as follows:

$$\cos\theta^* = f_S(\cos\theta - 1) + 1 \tag{2}$$

where θ is the theoretical water contact angle which would be measured on a flat solid surface and f_S is the solid surface fraction. This relation clearly shows that high roughness or open porosity (small f_S) decreases the measured water contact angle, thus increases the surface hydrophilicity ($\theta^* \to 0$).

3.5.2. Experimental setup

The water contact angles are measured using a goniometer KRÜSS G10 (see Fig. 13) that is equipped with a system for image analysis. It consists of a CCD video camera, a card acquisition connected to a PC and the Drop Shape Analysis (DSA) software for image processing. Environmental chamber has constant temperature (20^{o}C) in it and, therefore, constant humidity to ensure that the water drop does not evaporate while measurements are done. A water droplet is deposited on the sample surface by the help of syringe with constant volume ($V_w \approx 1.5\mu L$) [10]. Cold light source creates a shadow-like pattern of the water droplet that is further captured by the CCD camera and analyzed with the DSA software. Several droplets are deposited on the surface of the sample for more statistical results.

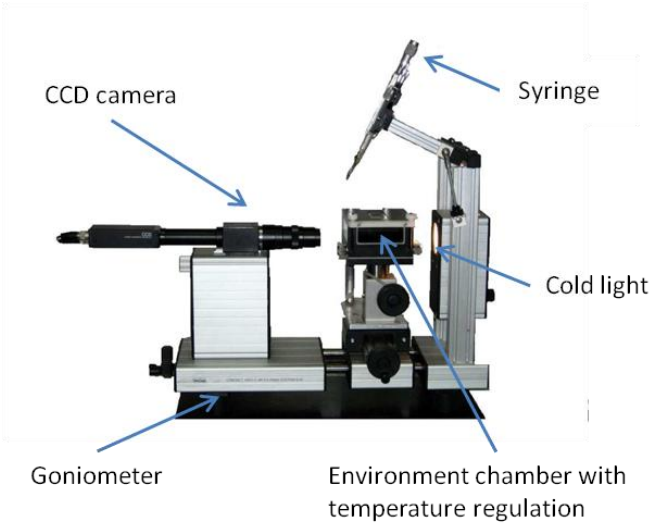

Fig. 13: Schema of the device for water contact angle measurements

4. Elaboration

As it was mentioned before, in this thesis work, our interest is to create a porous/rough structure in the TiO_2-SiO_2 composite material that would increase the natural super-hydrophilicity effect, i.e. increase the persistence of natural super-hydrophilicity over aging. For this reason, we have defined the basic system of the samples consisting of three layers: composite film, PS single-layer and impregnated composite layer.

4.1. Elaboration of TiO_2-SiO_2 composite films by sol-gel process

By sol-gel process one can elaborate a network of amorphous oxide via an inorganic polymerization reaction in liquid solution at ambient temperature. This technique allows the creation of thin films resulting from a liquid solution (sol) that, after the evaporation of solvent and thermal treatment, forms, respectively, a xerogel (inorganic polymer) film and an inorganic (oxide) film (see Fig. 14).

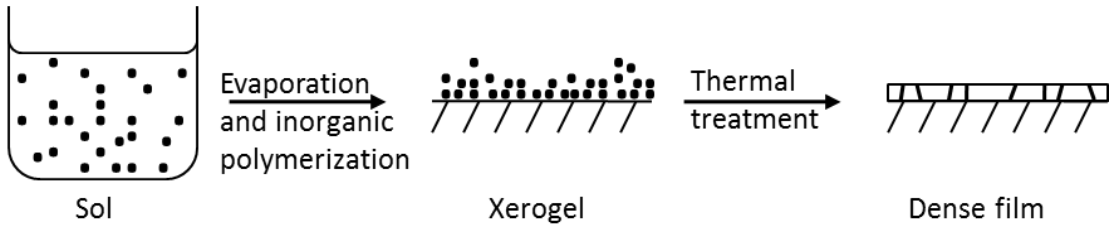

Fig. 14: Formation of thin films via sol-gel approach

With $M(OR)_n$ group as an alkoxide type precursor, where M is a metal and R is an alkyl radical, inorganic polymerization is based on the following reactions:

1. Hydrolysis: $M(OR)_n + H_2O \rightarrow OH\text{-}M(OR)_{n-1} + ROH$
2. Condensation:
    a) Oxolation, in case of water liberation:
    $(OR)_nM\text{-}OH + OH\text{-}M(OR)_n \rightarrow (OR)_nM\text{-}O\text{-}M(OR)_n + \mathbf{H_2O}$
    b) Alkoolation, in case of alcohol liberation:
    $(OR)_nM\text{-}OH + OR\text{-}M(OR)_n \rightarrow (OR)_nM\text{-}O\text{-}M(OR)_n + \mathbf{ROH}$

Both hydrolysis and poly-condensation reactions progress simultaneously in solution. It leads to polymeric inorganic chains that develop an inorganic network after liquid film deposition. The reactivity of sol-gel solutions (length and degree of cross-linking polymer chains formed from sol-gel reactions) can be controlled by various factors such as concentration of reactants (alkoxide, water) and addition of acidic or basic catalyst. These parameters were studied previously in the work of M. Houmard et al. [10]. In this work, the sol-gel principles were adapted to activate the reactive mechanisms in liquid solution in order to form inorganic TiO_2 nano-crystallites in suspension, which could be then diluted in a polymeric silica sol.

4.2. Elaboration of TiO_2-SiO_2 composite sols

TiO_2-SiO_2 composite sols are prepared by mixing a TiO_2 crystalline suspension (CS) with a SiO_2 sol in various molar ratios.

4.2.1. Crystalline suspension of TiO_2 (CS)

A crystalline suspension (CS) of anatase phase TiO_2 is prepared from a mother solution (MS) of polymeric TiO_2. To prepare MS, tetraisopropylorthotitanate (TIPT) is mixed with distilled water and hydrochloric acid and using absolute ethanol as solvent [25]. TIPT concentration in the solution is 0.4M and the molar ratio of TIPT/H_2O/HCl is 1/0.82/0.13. Then, before usage, solution is aged for two days in ambient temperature. A multi-step procedure, developed in LMGP [26,27], is then applied to elaborate a CS from the MS. The MS is firstly diluted in high amount of deionized water (molar ratio of H_2O/TIPT is 90) and autoclaved at 130^{o}C for 6 hours. Autoclaving process leads to the crystallization of TiO_2 nanoparticles of anatase phase diluted in aqueous medium. This crystallization, resulting from sol-gel reactions in aqueous and acidic conditions, relies on an activation of the hydrolysis reaction and slowing down of the poly-condensation reactions via peptization mechanisms. Nucleation of anatase TiO_2 follows from the pure oxide clusters formed during the process described previously. An exchange procedure is performed in order to remove the water from the sol and replace it with absolute ethanol. The final concentration of TiO_2 in ethanol is 0.24M and the CS is composed of nano-particles crystallized in the anatase phase with a diameter of about 5-6 nm [6]. Previous studies have shown that these conditions lead to very stable suspensions that can be used for several

weeks in order to elaborate pure TiO_2 coatings. In order to obtain TiO_2-SiO_2 composite sols, one can mix the CS with a polymeric solution of SiO_2.

4.2.2. Polymeric solution of SiO_2 (S1) and TiO_2-SiO_2 composite films

A sol of SiO_2 is prepared by diluting tetraethoxylane (TEOS) in absolute ethanol, distilled water and hydrochloric acid [28]. First, a solution in ethanol is elaborated with a TEOS concentration of 2.35M and a fixed H_2O/TEOS molar ratio (R_w) and pH. After, this sol is steamed at 60°C for 2 days. Finally, it is diluted in absolute ethanol till the desired concentration is obtained. The sol can then be mixed with a CS to form a TiO_2-SiO_2 composite sol. It is worth mentioning that the TEOS concentration, R_w ratio, and pH strongly influence the SiO_2 sol reactivity. Increasing this sol-gel reactivity will in turn induce long Si-O-Si polymer chains that form the network of SiO_2. In his thesis, M. Houmard has shown that this sol reactivity strongly impacts the physicochemical and morphological properties of composite layers, which in turn strongly influence their hydrophilic properties [10]. Accordingly, sols of weaker reactivity leading to very short SiO_2 polymeric chains were observed to favor a greater number of Ti-O-Si interfaces in TiO_2-SiO_2 composite films, which promoted enhanced super-hydrophilic properties, i.e. an enhanced persistence of the natural super-hydrophilicity. In the present work we wanted to assess in which extent an increased roughness or porosity could enhance the super-hydrophilicity of composite films. For this reason, we have chosen to study composite film of rather weak super-hydrophilicity persistence in order to better assess morphology effects. Thus, composite films were deposited from a sol of rather strong reactivity based on a TEOS concentration of 1.5M, a R_w ratio of 2.2 and a pH of 3.5. This sol was then mixed with the CS in various proportions. We have been interested in two different composites with 20mol% (which will be noted S1-20) and 60mol% (S1-60) of SiO_2. Pure TiO_2 (S1-0) and SiO_2 (S1-100) films have also been deposited from the CS and SiO_2 sols, respectively.

4.3. Elaboration of TiO_2-SiO_2 composite films

When the composite sols with desired compositions (S1-0, S1-20, S1-60 and S1-100) were obtained, we used the spin-coating method to elaborate the composite layers. For this purpose, standard parameters were applied: liquid volume of 300µL, rotation speed of 3000rpm, duration of rotation of 1s, acceleration of 5000rpm/s. Obtained samples were

heated at 500^{o}C for 2 hours to ensure the complete evaporation of the solvent and densification of the film.

This protocol was used to impregnate previously deposited PS films. It was also used to deposit TiO_2-SiO_2 super-hydrophilic films in order to compare how the super-hydrophilicity influences the deposition of PS films compared to a bare silicon substrate.

5. Results and discussion

5.1. Elaboration of polystyrene (PS) films

As the spin-coating deposition of layers composed of polystyrene latex beads (purchased from *Sigma – Aldrich Chemie GmbH*, Germany) relies on numerous parameters, one has first to study and define the best deposition conditions and suspension preparation parameters leading to closely packed PS beads. This optimization work is described in the next sections.

5.1.1. Deposition conditions

The purpose is to define experimental conditions in order to obtain 2D layers of closely packed polystyrene latex beads with an average diameter $d = 0.6\mu m$. PS beads are supplied as aqueous suspensions of 10wt% concentration. The colloidal solution in water was diluted in solvent in volume proportion 1:9 obtaining a 1wt% PS colloidal suspension. Theoretical calculations were done to preliminary define the deposition volume necessary to totally cover a substrate (silicon) of dimensions $3\times3cm^2$ with closely packed (square arrangement) PS beads, taking into account the solution concentration of 1wt%. The deposition volume was thus initially fixed at $V = 50\mu L$.

Several manipulations (*M*) with different conditions were then performed 'step-by-step' in order to optimize the protocol for PS single-layer elaboration on silicon.

5.1.1.1. M1: Standard protocol and influence of solvent

First, the standard protocol habitually employed to deposit composite films (3000rpm, 1s of rotation, 5000rpm/s) was tested with two different PS solutions dissolved in absolute ethanol (EtOH) or H_2O.

Optical microscope pictures show that one can obtain similar structures for both solvents: EtOH and H_2O (see Fig. 15). FEG-SEM images show that, although forming small domains and still having a lot of large 'free' spaces (i.e. uncoated substrate areas), one can obtain 2D arrangements of closely packed PS beads with both liquids. However, macroscopic observations show that water does not wet correctly the surface of Si substrate. As a result, further experiments were carried by using EtOH as a solvent. Besides, although the wetting of a PS/EtOH solution was good, the substrate was poorly

covered at the macroscopic level (coverage rate of around 20%). Therefore other experimental conditions were tested in following manipulations.

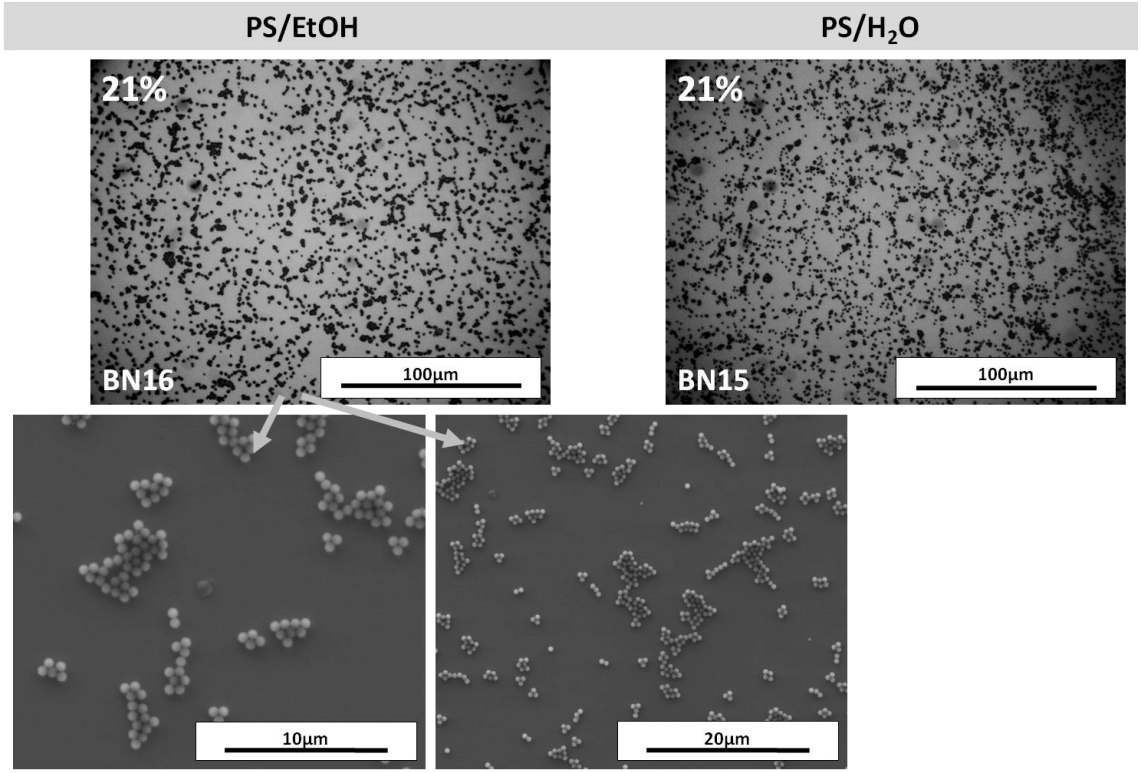

Fig. 15: Optical (top) and FEG-SEM (bottom) images representing the influence of solvent by using a standard deposition protocol (3000rpm, 1s of rotation, 5000rpm/s). The percentage indicated in optical images corresponds to the coverage rate

5.1.1.2. M2: Effect of the rotation speed and time

Secondly, the effect of the rotation speed and time were tested by combining three different rotation speeds (1000, 3000 and 5000rpm) and three different rotation times (1, 10 and 30s) while keeping the acceleration at 5000rpm/s (see Fig. 16).

Observations show that the best combination that leads to a higher coverage rate (around 50%) can be obtained with a small rotation speed for a short deposition time. Thus, next experimental conditions were defined: 1000rpm, 1s of rotation. To verify the lower limit of the rotation speed, a 500rpm speed was also tested. The results show that, although a decrease of the rotation speed considerably increases the coverage of the surface (up to 95%), it yields the formation of multi-layers of PS beads when using a silicon substrate. It was thus concluded that the choice of a rotation speed of 1000rpm was adequate and suitable for further experiments on silicon.

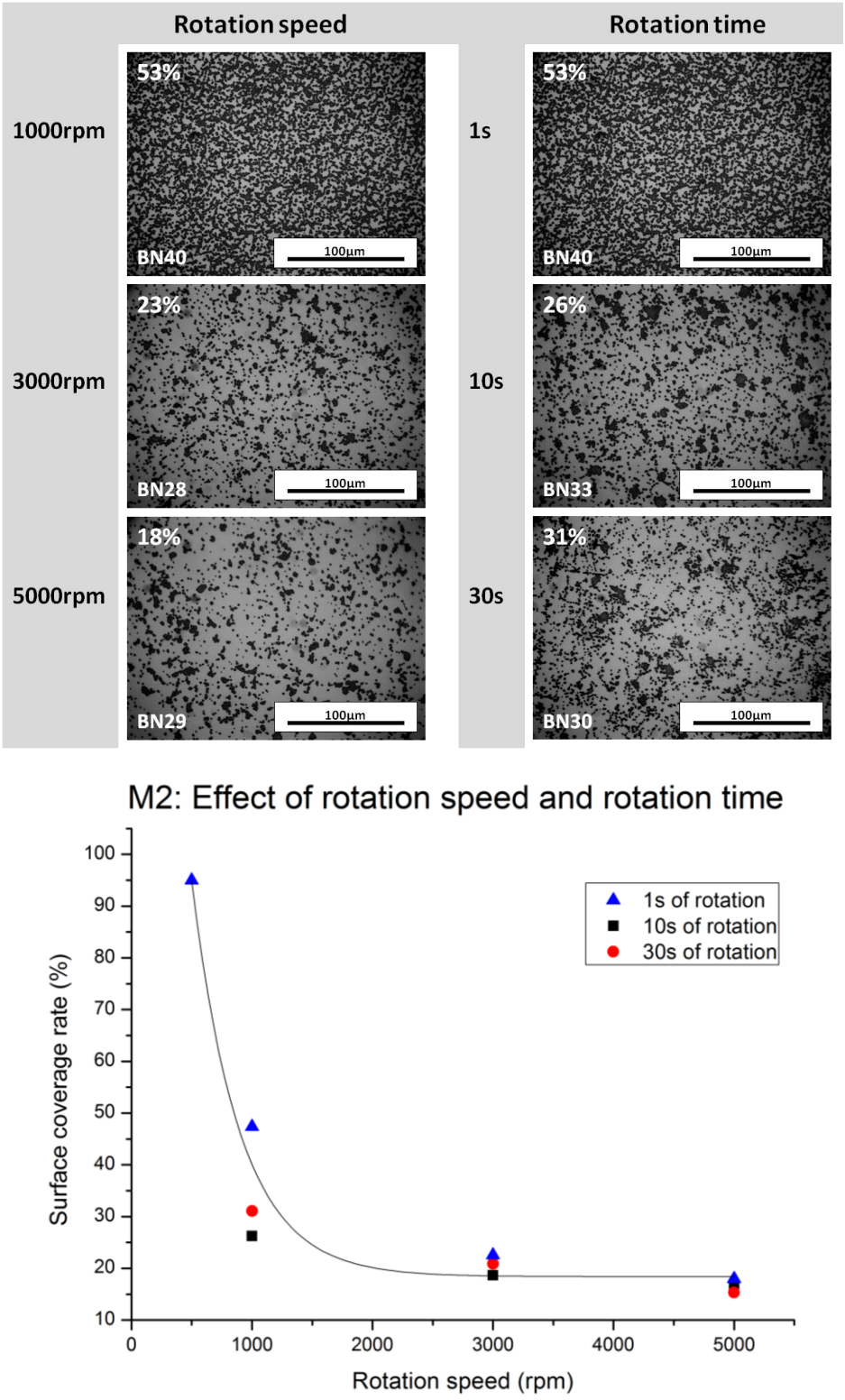

Fig. 16: Optical images and graphics represent results of different rotation speeds (1000, 3000 and 5000rpm) and rotation times (1, 10 and 30s) tested with 1wt% PS solution in EtOH. The percentage indicated in optical images corresponds to the coverage rate, whose values are plotted in the above curve as a function of studied rotation speeds and times

5.1.1.3. M3: Acceleration of the turning plate

When studying the work of Colson et al. [19], one can see that single-layers of closely packed PS beads are favored by a long acceleration step in the spin-coating parameters to improve the coverage rate. To assess this effect, tests were performed with a rotation speed of 1000rpm and various accelerations on bare Si substrate. 5000rpm/s was chosen as the highest and 100rpm/s as the lowest value of acceleration (see Fig. 17).

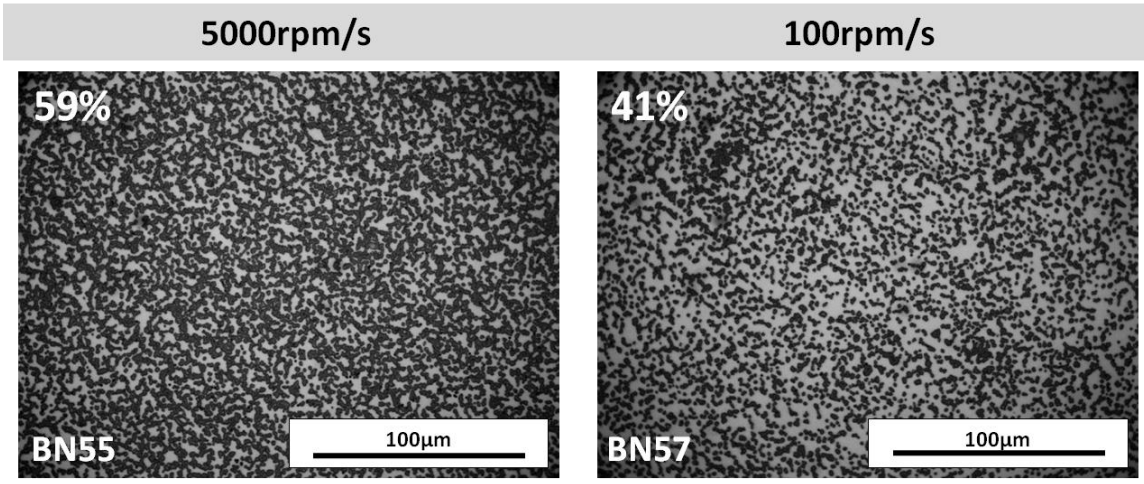

Fig. 17: Optical images representing the influence of the surface coverage when different accelerations are applied: 5000rpm/s (left) and 100rpm/s (right). The percentage indicated in optical images corresponds to the coverage rate

Contrary to the work of Colson et al. [19], our results show that a better surface coverage is obtained with a higher value of acceleration. Thus, 5000rpm/s acceleration was definitively adopted for next experiments.

5.1.1.4. M4: Reproducibility

The reproducibility of our protocol was tested on bare silicon substrates for different experiments in fixed conditions: 1000rpm, 1s of rotation, 5000rpm/s. In these conditions it can be shown that it is possible to reasonably reproduce PS single-layers with an average coverage of 53 ± 6%. Results are confirmed also by the FEG-SEM observations (see Fig. 18).

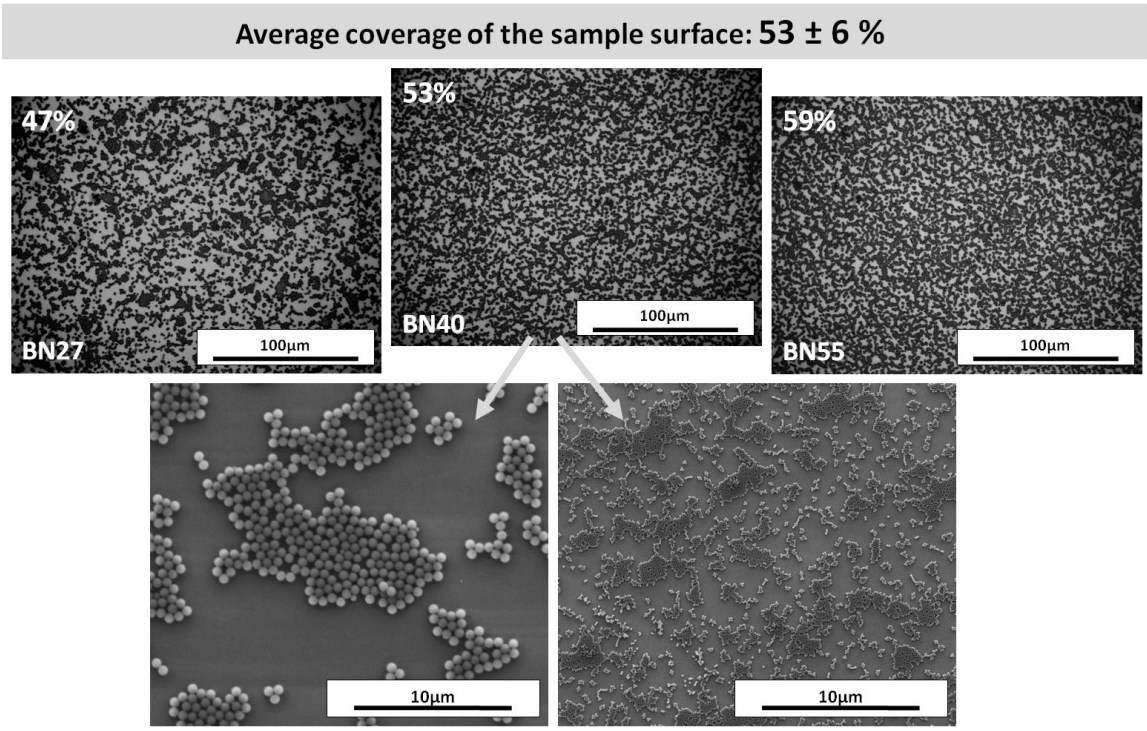

Fig. 18: Reproducibility of the samples represented by optical (top) and FEG-SEM (bottom) images. The percentage indicated in optical images corresponds to the coverage rate

5.1.1.5. M5: Influence of the magnetic agitation and ultrasonic treatment

When technical conditions, related to spin-coating settings, are defined, another factor that might influence the coating quality and reproducibility is the dispersion and stability of PS beads in the liquid solution. In this case two mixing methods were tested: magnetic agitation (MA) and ultrasound dispersion (US). We chose four different timings for US (5', 30', 1h and 2h), and five timings for MA (5', 1h, 4h, 6h and 23h) for a 1000rpm rotation speed (see Fig. 19). A longer duration of magnetic or ultrasonic agitation leads to a slight increase of the coverage rate. However, one can consider that this influence is relatively weak. For this reason, a magnetic agitation of two hours has been defined as the optimal conditions for solution preparation.

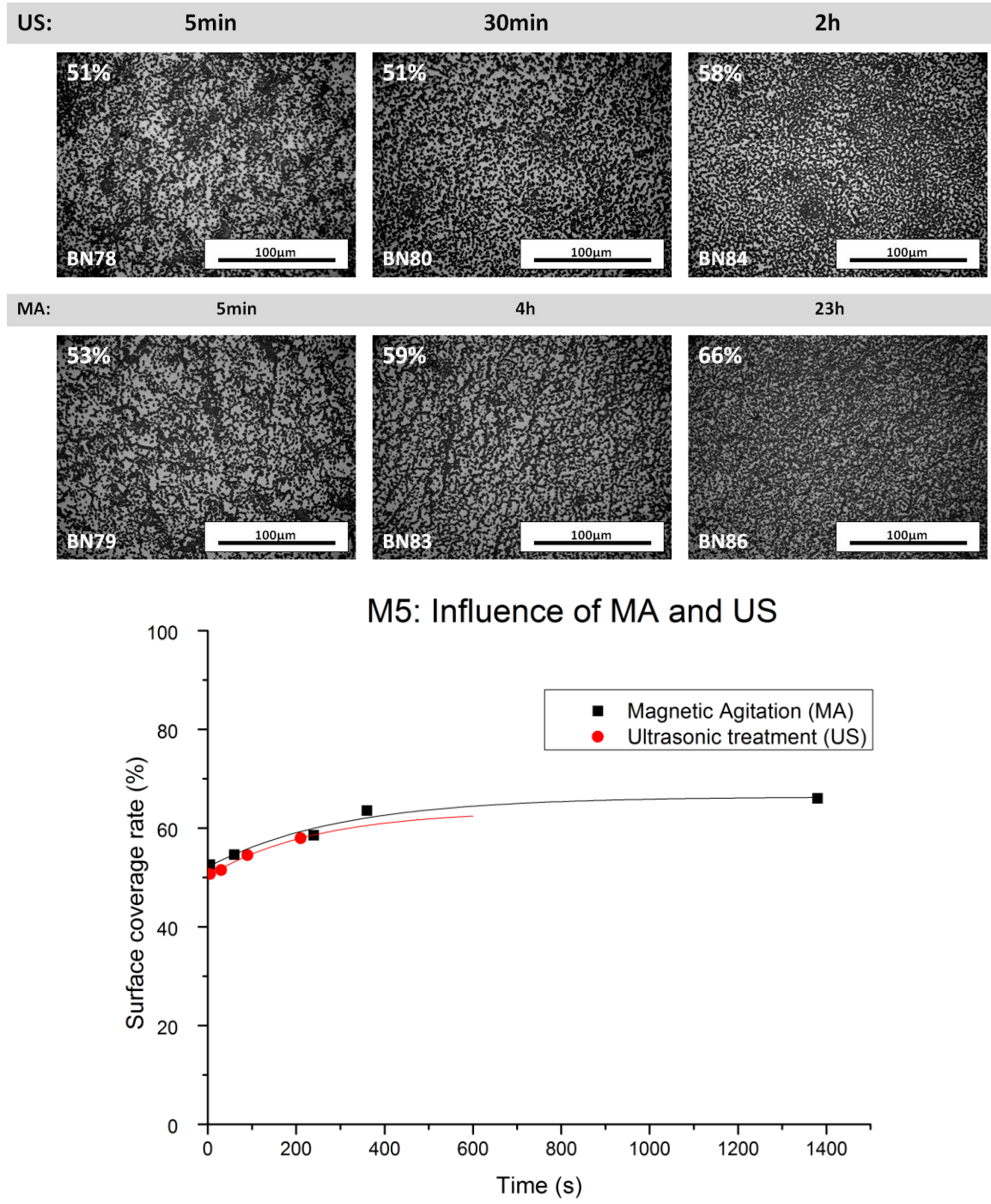

Fig. 19: Influence of the duration of the ultrasound (US) and magnetic agitation (MA) represented by optical images and graphics. The percentage indicated in optical images corresponds to the coverage rate, whose values are plotted in the above curve as a function of studied US and MA durations

5.1.1.6. M6: Influence of the substrate

We also assessed how the substrate hydrophilicity could influence the deposition of PS beads. For this purpose, tests were performed on a silicon substrate preliminary coated with a super-hydrophilic composite film and rotation speeds of 500rpm and 1000rpm.

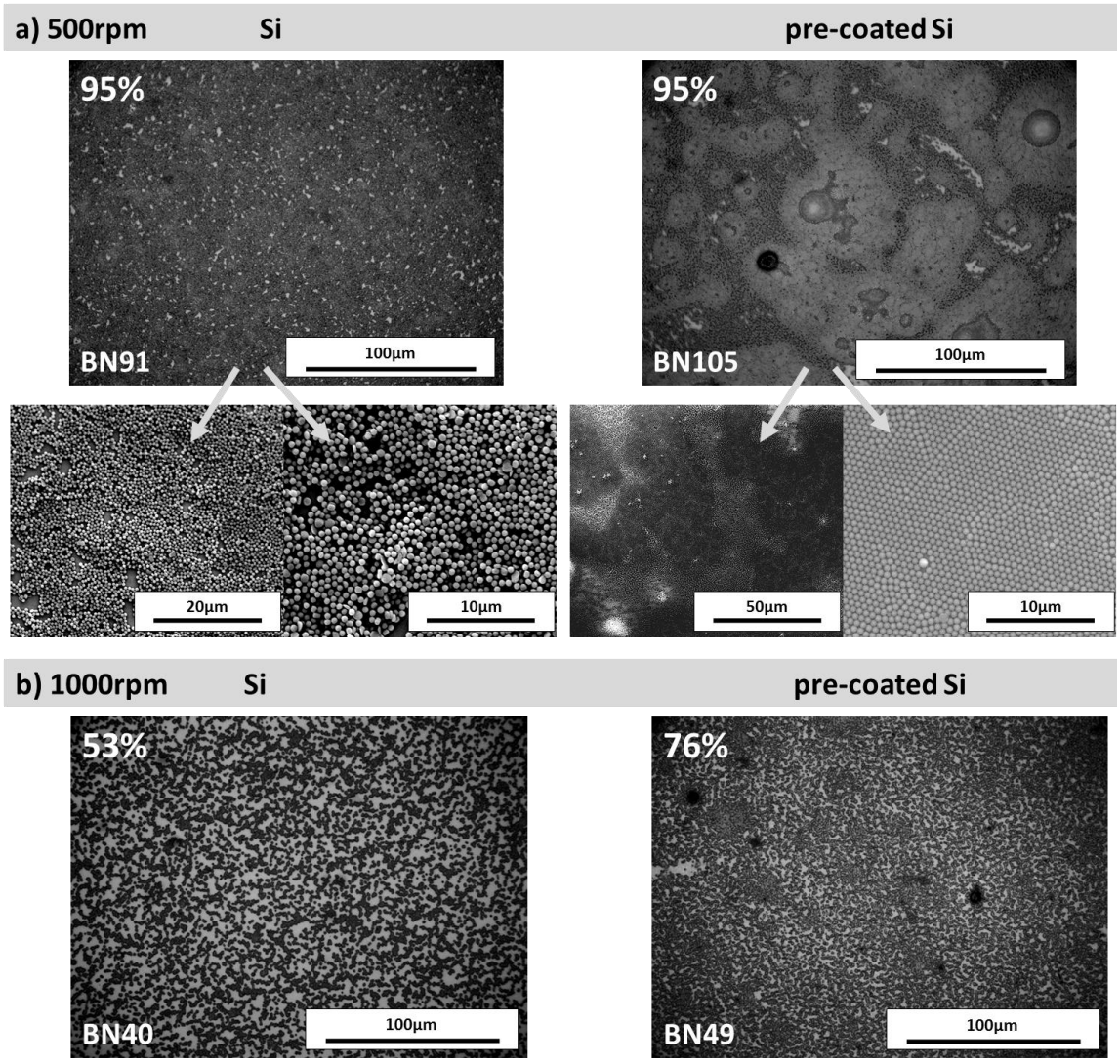

Fig. 20: (a) Optical (top) and FEG-SEM (bottom) images representing the influence of a rotation speed of 500rpm tested on different surfaces: bare Si (left) and Si pre-coated with super-hydrophilic film (right); (b) Optical images representing the influence of a rotation speed of 1000rpm tested on different surfaces: bare Si (left) and Si pre-coated with super-hydrophilic film (right)

Fig. 20 shows that the substrate influence strongly depends on the speed rotation:

1) ***500rpm***: A strong coverage rate (around 95%) is obtained whatever the substrate hydrophilicity. However, in contrast to a bare Si substrate (section 5.1.1.2), in the case of a pre-coated substrate the multi-layer formation is observed only in some localized regions where particle aggregates are formed, and the major part of the substrate is covered with an aggregate-free 2D layer of closely packed PS particles (see Fig. 20a).
2) ***1000rpm***: A 2D layer of closely packed PS particles is obtained whatever the substrate hydrophilicity. However, compared to a bare Si substrate, the pre-deposition of a super-hydrophilic coating strongly enhances the coverage rate from about 50% to about 75% (see Fig. 20b).

Thus, these observations open the way to different options of PS particle coatings for the subsequent impregnation of composite sols.

5.1.2. Parameters for suspension preparation

Once the technical (spin-coating) parameters and deposition conditions are better determined, one has to improve and determine the parameters of the solution preparation that influence the surface coverage. New studies (*NS*), performed on bare Si substrates, are discussed in the following sub-sections.

5.1.2.1. NS1: Influence of concentration

First of all, different concentrations of PS in EtOH were tested. Different dilution rates of the initial 10wt% PS solution in water were chosen: dilution by a factor 0, 2, 5 and 10 that corresponds, respectively, to solutions with a 10, 5, 2 and 1wt% concentration. Deposition on both, bare Si and Si substrates coated with a super-hydrophilic film were performed for 1000rpm rotation conditions (see Fig. 21).

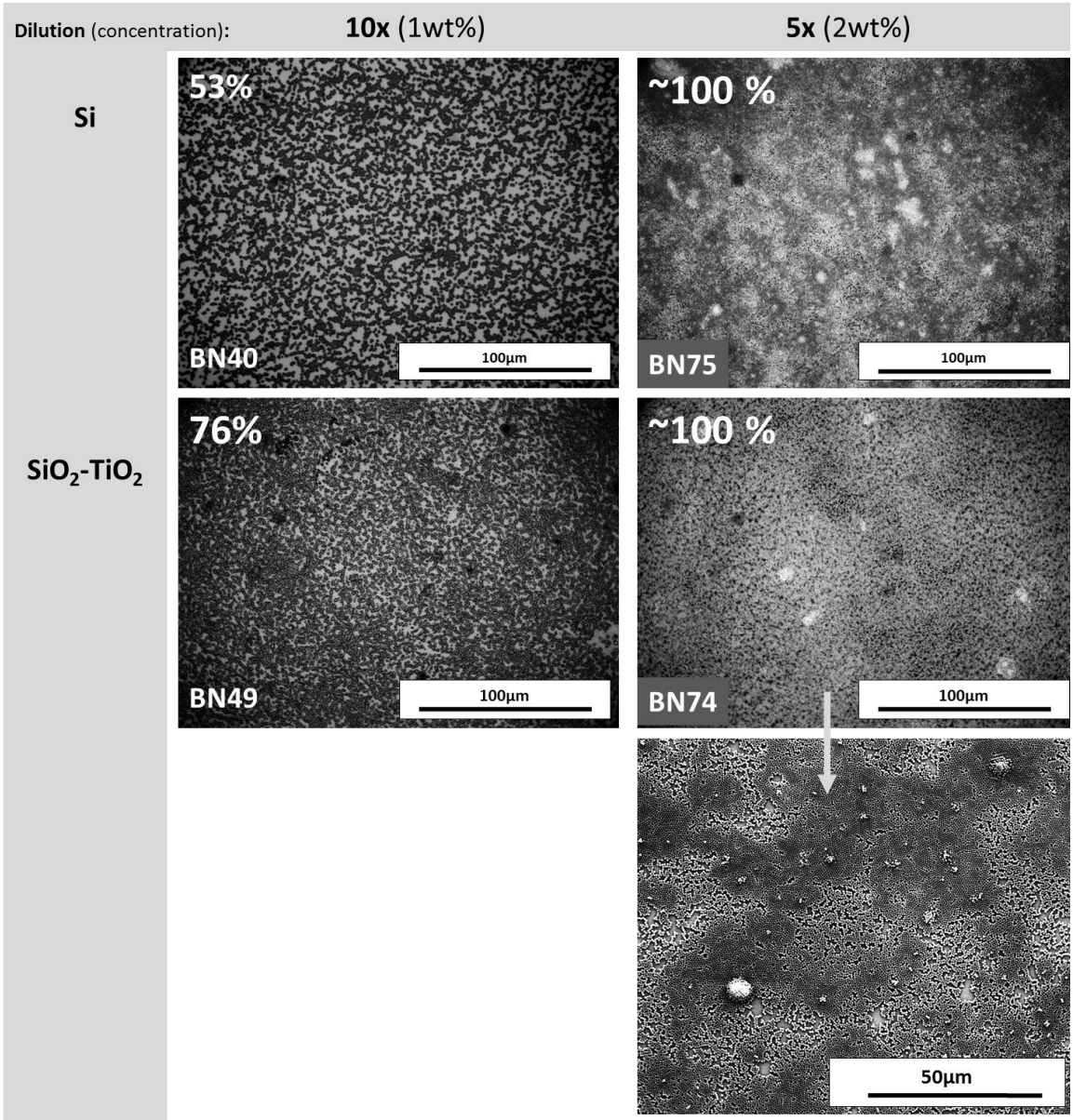

Fig. 21: Influence of the PS solution concentration represented by optical (top, middle) and FEG-SEM (bottom) images. The percentage indicated in optical images corresponds to the coverage rate

The observations show that a quasi-complete surface coverage can be obtained already with a PS concentration of 2wt% whatever the substrate hydrophilicity. However, one starts to observe the formation of rather inhomogeneous multi-layer regions that are not necessarily favorable to the objective of the work: post-impregnation of a composite sol. Therefore a PS concentration of 1wt% was definitely retained for further studies.

5.1.2.2. NS2: Influence of deposited volume

Another parameter to be assessed is the volume of deposited solution, so that the layer covers the whole substrate. Four values of deposition volume were chosen: 50, 100, 250 and 500µL for a bare Si substrate coated at 1000rpm with a 1wt% solution (see Fig. 22).

As a result, when observed with OM, one can see that the coverage rate does not depend significantly on the deposited volume (see Fig. 22a). However, macroscopic observations show that the substrate is completely covered when the deposition volume is V = 100µL (see Fig. 22b). Accordingly, V = 100µL has been defined as the deposition volume of the PS/EtOH solution (instead of the calculated volume, V = 50µL, used in previous studies).

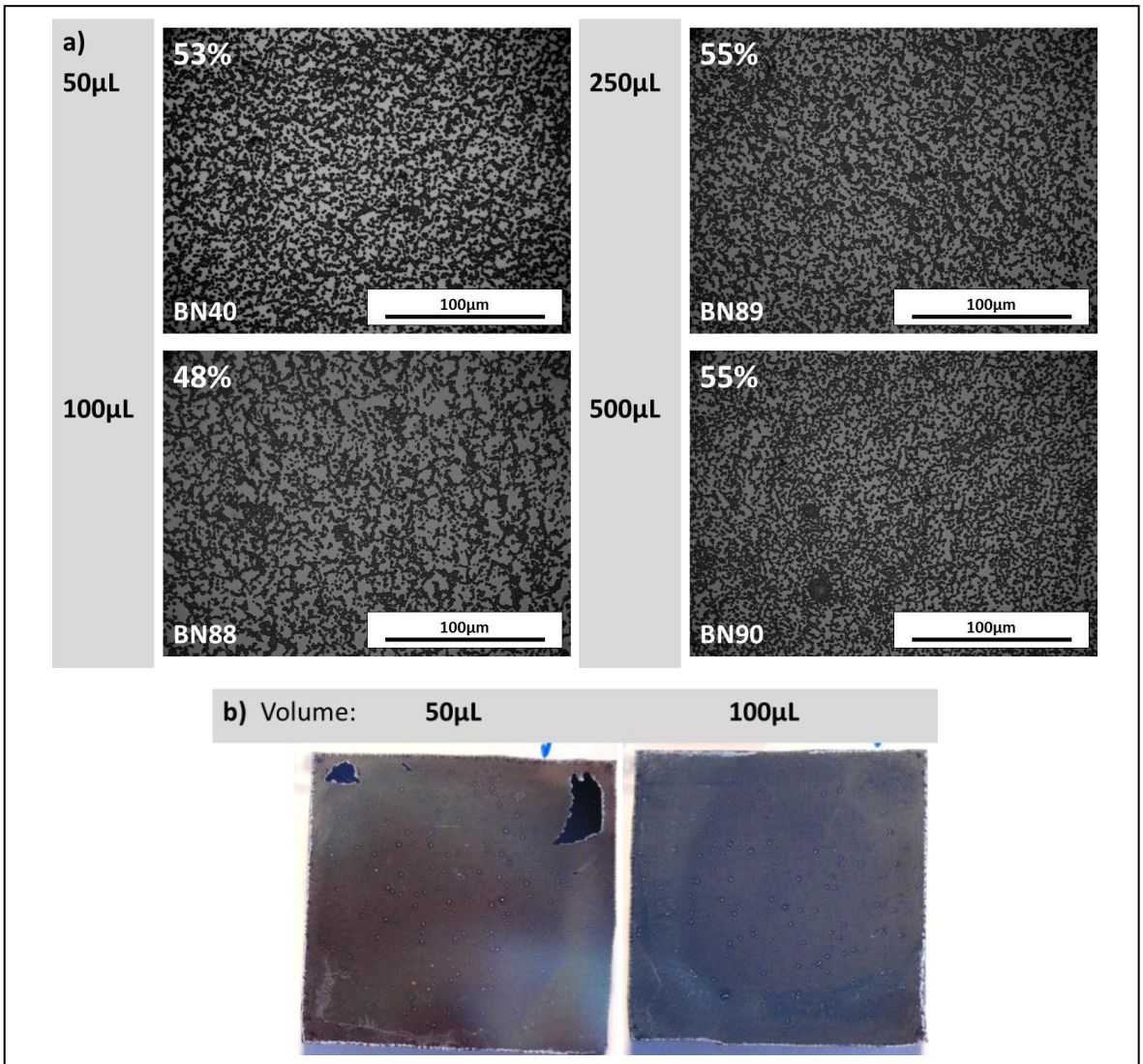

Fig. 22: Influence of the deposited volume of the solution (on Si substrate) observed in (a) microscopic scale with OM and (b) comparison of two samples in macroscopic scale. The percentage indicated in optical images corresponds to the coverage rate

5.1.3. Conclusion: Model conditions

Finally, one can summarize this experimental work by model conditions yielding most promising results to obtain PS 2D layers on bare Si substrates as well as on hydrophilic pre-coated substrates (see Table 1). These model conditions will be used for following studies.

Table 1: Summary of model conditions to obtain PS 2D layers

Condition	Value
Deposition volume	100µL
Rotation speed	500rpm or 1000rpm
Duration of rotation	1s
Acceleration	5000rpm/s

Besides, owing to better results obtained on hydrophilic substrates, we have chosen this option in the following parts of this work. Accordingly, PS 2D layers were deposited on sub-layers of four different composite materials: S1-0 (pure TiO_2), S1-20, S1-60 and S1-100 (pure SiO_2). Composite sub-layers were deposited as described in section 4.3. After deposition of PS beads, samples were placed for 5 min into a furnace at 110^{o}C to ensure the complete evaporation of the solvent and better attachment of PS beads onto the sub-layer. Then, the bi-layer samples were impregnated with a composite sol with a composition identical to that of the sub-layer. This impregnation was done by spin-coating in conditions used for sub-layer deposition (section 4.3). After impregnation, the samples were placed for 2 hours in a furnace at 500^{o}C to ensure the calcination of PS particles and subsequent creation of a porous/rough structure in the composite films.

5.2. Study of PS + composite multilayer films

5.2.1. Preliminary observations

Preliminary experiments of impregnation were done with a S1-60 TiO_2-SiO_2 composite sol. The samples were observed by optical microscopy, first of all just after deposition of PS beads at 1000rpm on a super-hydrophilic sub-layer, and then after post-impregnation of the composite sol and thermal treatment. As well, FEG-SEM characterization was done to verify the surface structure and obtain information on the morphologic characteristics of the samples (see Fig. 23).

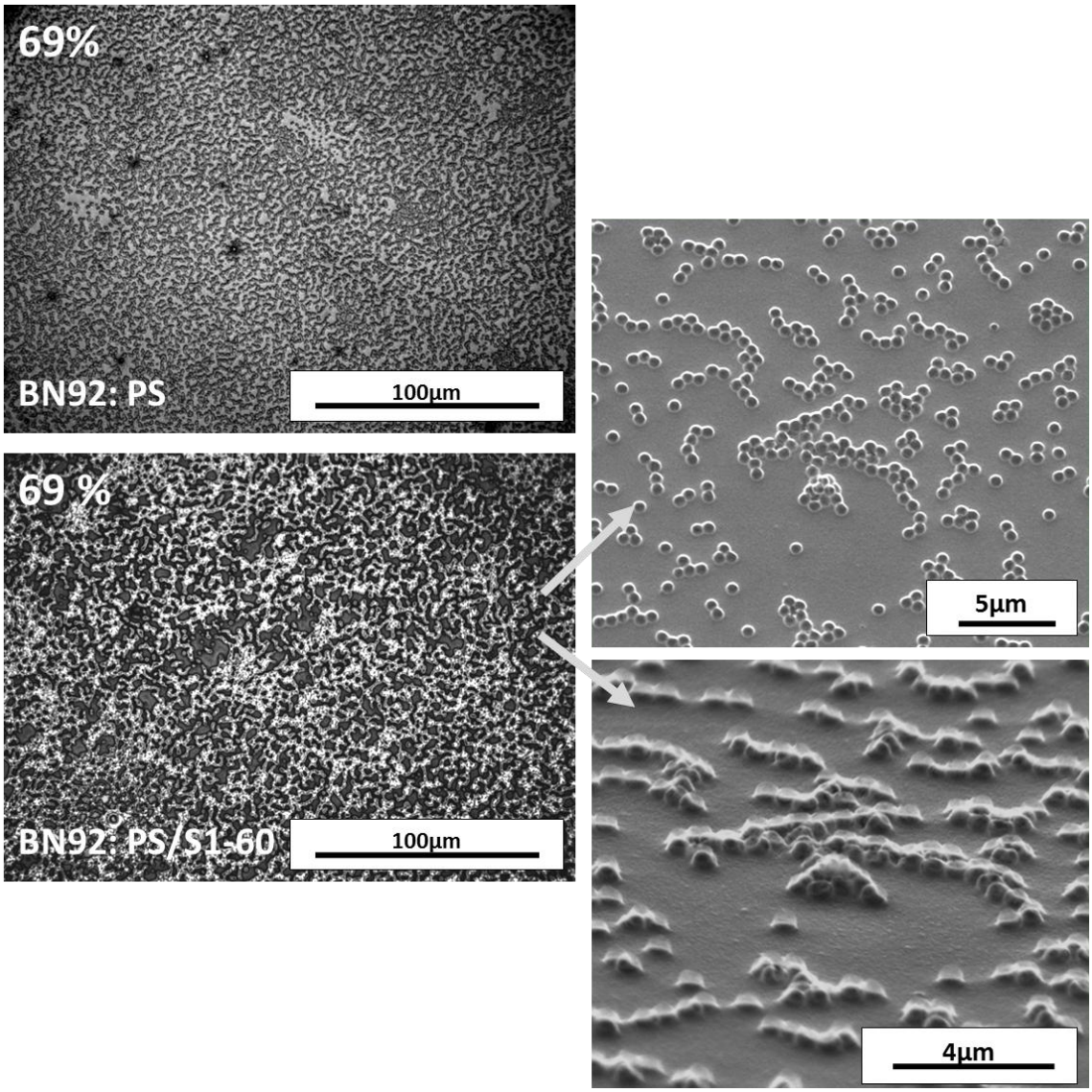

Fig. 23: Optical (left) images characterizing samples before (top) and after (bottom) impregnation with hydrophilic TiO_2-SiO_2 composite S1-60. The FEG-SEM images (top view and tilted sample view) on right illustrate morphology of a composite coating after post-impregnation. The percentage indicated in optical images corresponds to the coverage rate

As it is seen from Fig. 23, after impregnation and thermal treatment (2h at 500^{o}C) is done, one can observe that the pattern of PS layer is maintained, i.e. the coverage rate. FEG-SEM images show that the composite material enrobes the PS beads and, after calcination, the composite material adopts a particulate morphology with a geometry very similar to that of the initial PS coating, which probably suggests that the composite coating exhibits a porous shell-like structure. This structure would arise from the capping of previously deposited PS beads by the composite sol, followed by the burning out of PS beads during calcination.

The next try was to test the impregnated volume of composite sol. The previously defined volume 300µL was increased 2 and 3 times: 600µL and 900µL, respectively. As it is seen in Fig. 24, the increase of the composite sol volume for the impregnation layer does not change significantly the morphology of the composite surface. Thus, the volume for impregnations was defined as $V_{comp} = 300\mu L$ for further experiments.

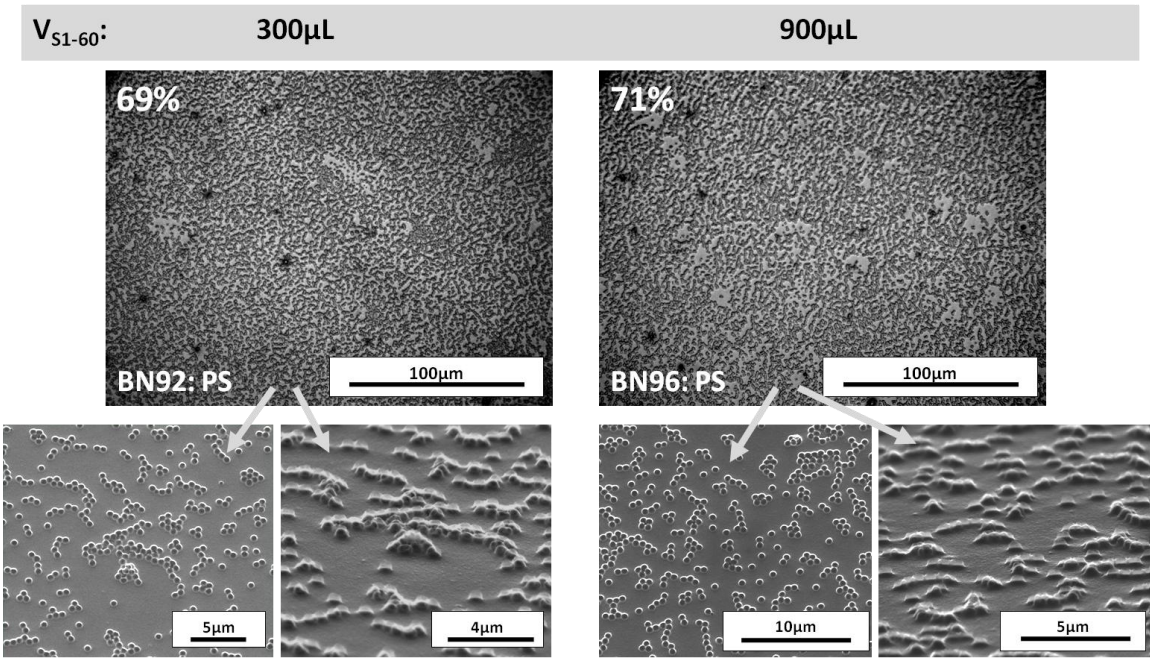

Fig. 24: Optical images (top) representing different composite impregnation volumes and FEG-SEM images (bottom) representing the surface morphology after impregnation of the composite sol (top view and tilted sample view). The percentage indicated in optical images corresponds to the coverage rate

5.2.2. Study of reference composite films

Reference composite films directly deposited on Si substrates without PS beads were then investigated. Roughness of the surface was studied by FEG-SEM and AFM and characterized by RMS (Root Mean Square, measured in *nm*) function. Fig. 25 shows that the surface roughness of reference S1-0, S1-20 and S1-60 composite films are as follows: $RMS_{S1\text{-}0} = 4.8nm$, $RMS_{S1\text{-}20} = 4.6nm$ and $RMS_{S1\text{-}60} = 3.6nm$. No roughness could be measured on a S1-100 film, which indicates a very smooth surface of the pure SiO_2 film. As it is seen, the RMS values are not high in none of the cases.

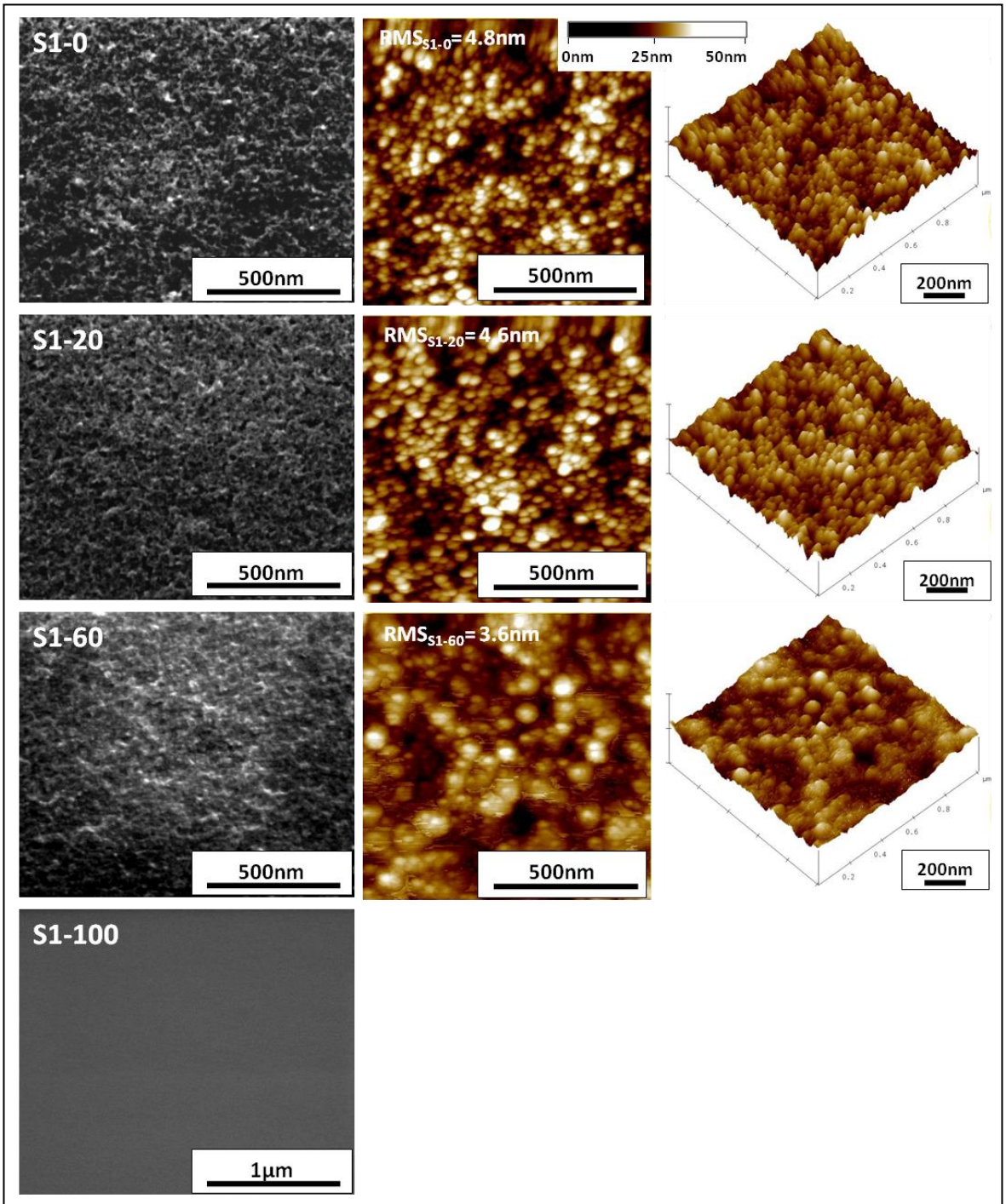

Fig. 25: FEG-SEM (left) and AFM (2D in middle, 3D on right) images to represent the morphology and roughness of composite films S1-0, S1-20, S1-60 and S1-100 directly deposited on Si substrates

The evolutions of water contact angle over aging of these reference films are illustrated in Fig. 26. It is observed that pure TiO_2 (S1-0) and SiO_2 (S1-100) films rapidly lose their initial super-hydrophilicity. In comparison, the super-hydrophilicity loss is slower for S1-20 and S1-60 composite films, which provides new illustration of the specific wettability properties of such films. However, compared to best films optimized in the thesis of M. Houmard, as illustrated in Fig. 2 and Fig. 3, the super-hydrophilicity loss of S1-20 and S1-60 films over aging is much faster in the present case. As explained before, it is due to the much greater sol-gel reactivity of SiO_2 sols chosen in the present work compared to the very weak reactivity of best sols optimized by M. Houmard. It should also be noticed that aging data illustrated in Fig. 26 exhibit some experimental dispersion and that pure TiO_2 (S1-0) films yield more dispersed wettability data over aging than other studied compositions. In agreement with previous studies performed at *LMGP*, this greater dispersion depicts that, compared to other compositions, pure TiO_2 films exhibit a greater sensitivity to fluctuations of the pollution conditions over aging, for example relative humidity and/or temperature variations of the room atmosphere.

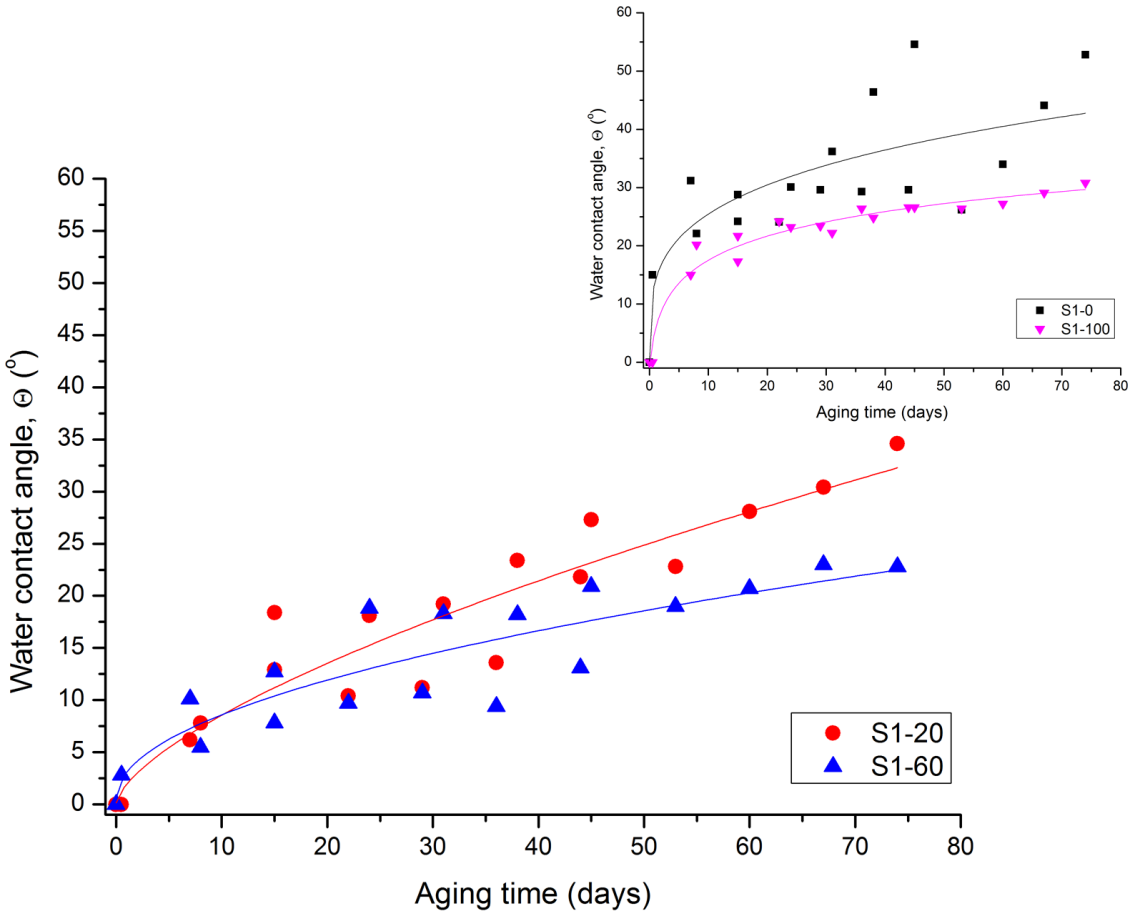

Fig. 26: Kinetics of water contact angle increase over aging for four different composite materials directly deposited on silicon without PS beads. The main figure compares the kinetics measured on S1-20 (●) and S1-60 (▲) films. The insert compares the same variations for S1-0 (■) and S1-100 (▼) films. For each composition, two series of samples were studied

In the following, we study how the pre-deposition of PS beads influences the roughness of composite coatings, and how roughness effects influence the wettability of such coatings compared to those directly deposited on silicon substrates without PS beads.

5.3. Morphology of PS + composite films

First of all, concerning PS beads deposition, one has to remind that two different experiments (with rotation speeds of 500rpm and 1000rpm) were held in parallel. As it was mentioned before, the morphology of samples was studied with FEG-SEM and AFM measurements and characterized by RMS function. Morphological characteristics arising from both studied rotation speeds for S1-0+PS, S1-20+PS, S1-60+PS and S1-100+PS composite films are summarized in Fig. 27, Fig. 28, Fig. 29 and Fig. 30, respectively.

5.3.1. Surface coverage

First of all, one can observe that the lower rotation speed (500rpm) yields higher surface coverage that is confirmed with both optical microscope images (threshold statistics) and AFM images. Optical images (see top pictures) show that well dispersed coated regions constituted of homogeneous particles can be obtained with three composites: S1-0+PS, S1-20+PS and S1-60+PS. Meanwhile, in the case of composites S1-100+PS (pure SiO_2 with PS), the coverage rate is strangely weaker and one observes the formation of rather continuous coated areas coexisting with large zones without any coating. These observations are confirmed also by AFM images (compare middle images of Fig. 27 to Fig. 30). Particular features observed in case of the S1-100+PS composite films are not yet explained and further research must be done.

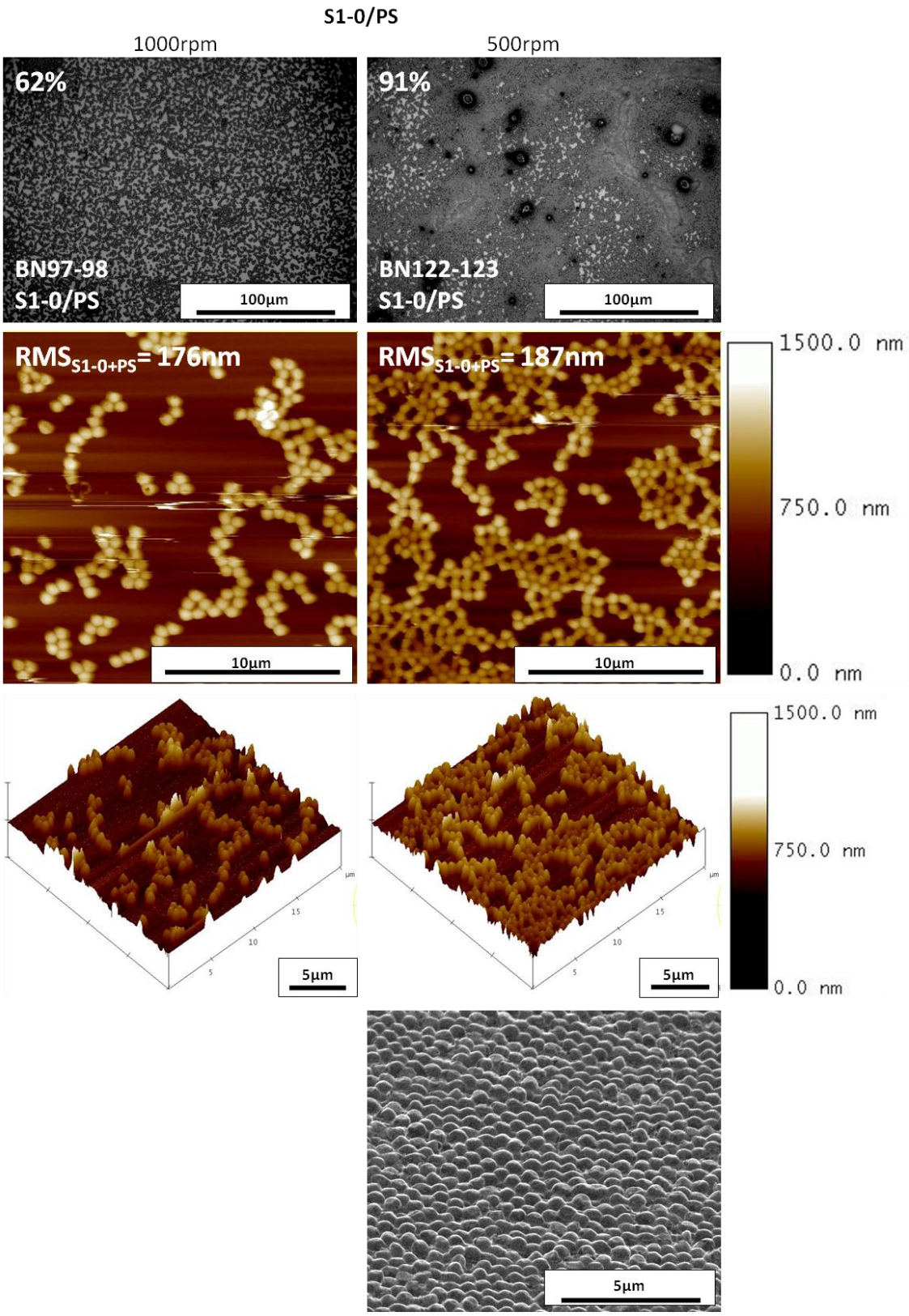

Fig. 27: Optical (top), AFM (2D and 3D in the middle) and FEG-SEM (bottom) images represent general and more detailed structures of S1-0 composite film. The percentage indicated in optical images corresponds to the coverage rate

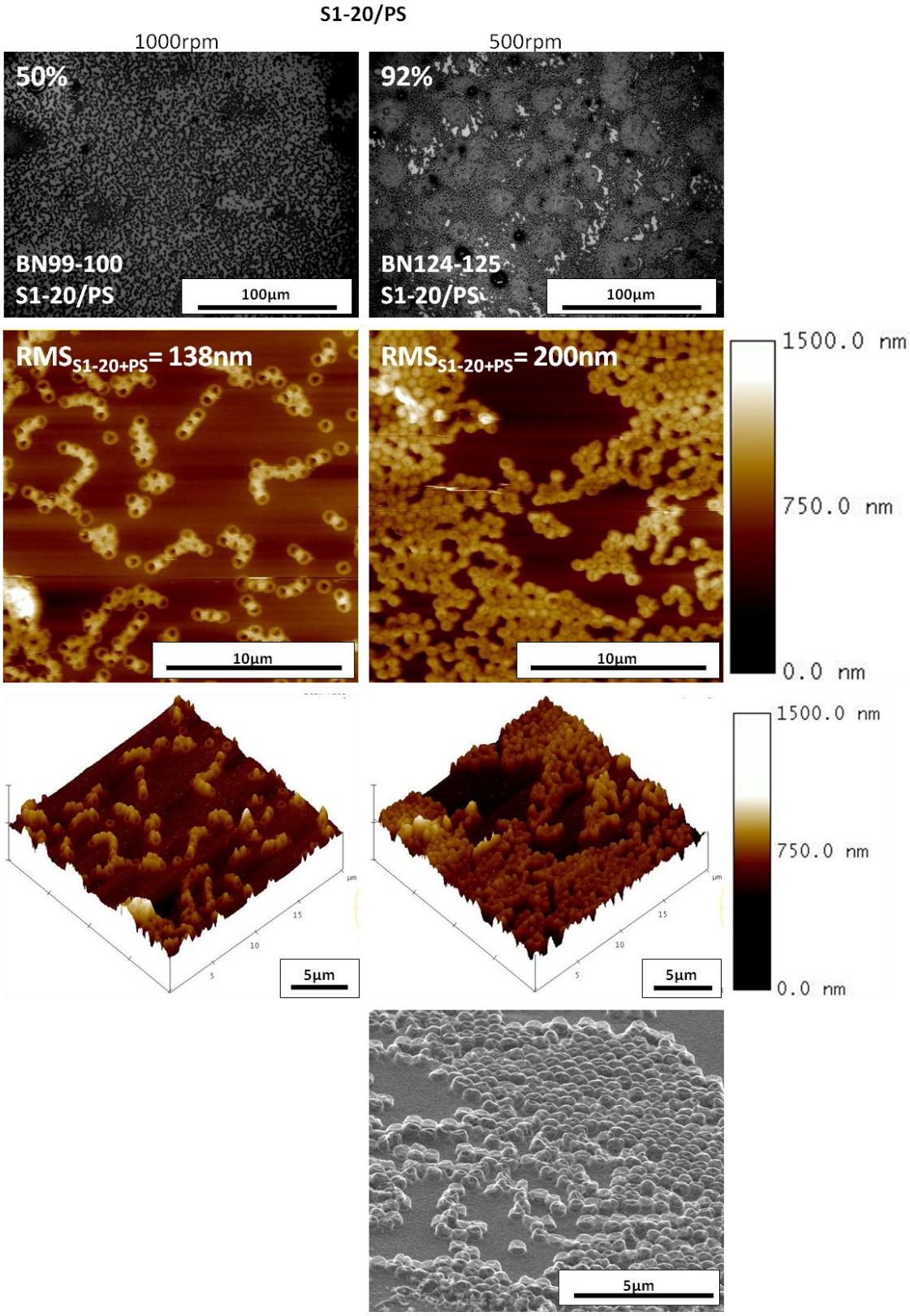

Fig. 28: Optical (top), AFM (2D and 3D in the middle) and FEG-SEM (bottom) images represent general and more detailed structures of S1-20 composite film. The percentage indicated in optical images corresponds to the coverage rate

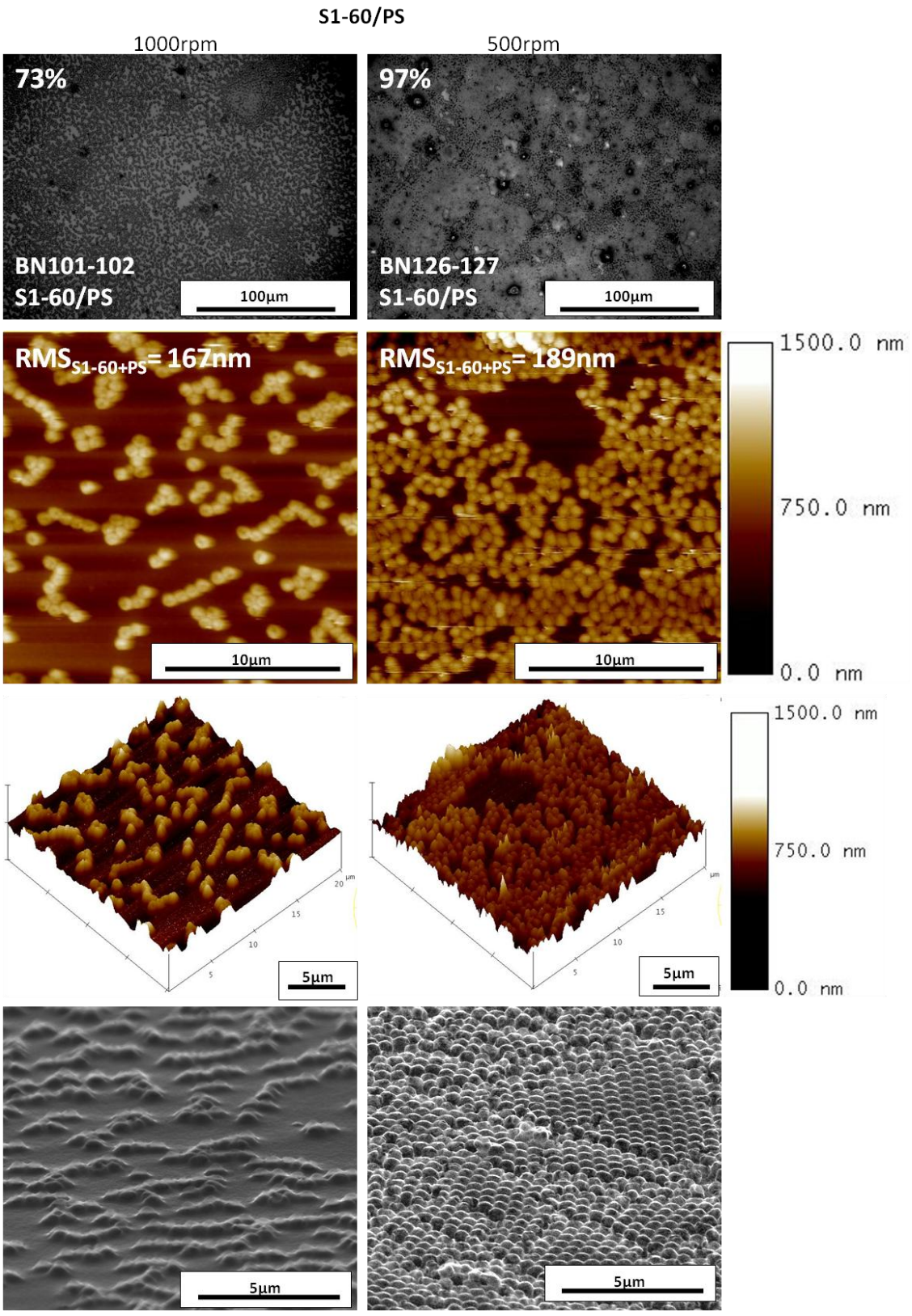

Fig. 29: Optical (top), AFM (2D and 3D in the middle) and FEG-SEM (bottom) images represent general and more detailed structures of S1-60 composite film. The percentage indicated in optical images corresponds to the coverage rate

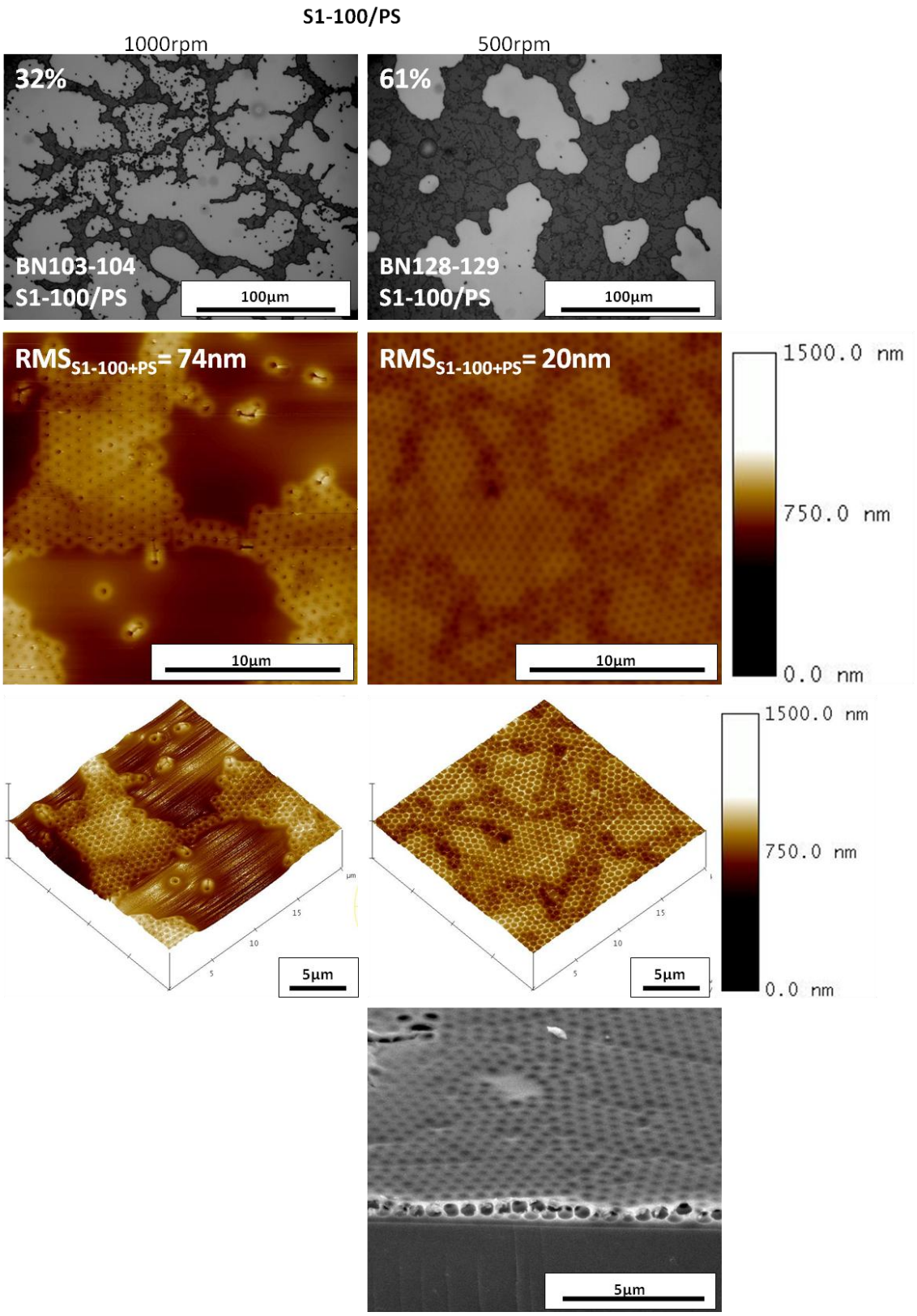

Fig. 30: Optical (top), AFM (2D and 3D in the middle) and FEG-SEM (bottom) images represent general and more detailed structures of S1-100 composite film. The percentage indicated in optical images corresponds to the coverage rate

5.3.2. RMS Roughness

3D representations in AFM images (see the third row in Fig. 27 to Fig. 30) confirm that the roughness of the samples is considerably increased by composite impregnation on the 2D layer of PS nanoparticles in both experiments (with rotation speeds 1000rpm and 500rpm) comparing to pure reference composite films. All RMS roughness values are summarized in Table 2.

Table 2: RMS roughness values of composite films and composite + PS films of two experiments with different rotations speeds (1000rpm and 500rpm)

Composite	RMS value of composite films, nm	RMS value of composite + PS films, nm	
		1000rpm	500rpm
S1-0	4.8	176	187
S1-20	4.6	138	200
S1-60	3.6	167	189
S1-100	2.7*	74	20

*for comparison, this value is extracted from M. Houmard's thesis work [10]

As seen from data in Table 2, in the case of S1-0+PS, S1-20+PS and S1-60+PS composites, the deposition of a 2D PS beads layer before composite impregnation leads to an increase of the RMS value by about two orders of magnitude. In contrast, S1-100+PS films show much lower RMS values. In addition, while in cases of S1-0+PS, S1-20+PS and S1-60+PS composites the RMS value increases with the increase of the surface coverage rate, i.e. the decrease of the rotation speed, the RMS value of S1-100+PS composite films strongly decreases. On the one hand and as mentioned before, the results for S1-100+PS films are not yet clear and further research must be done. On the other hand, further attention must be paid to other three samples S1-0+PS, S1-20+PS and S1-60+PS, as illustrated in Fig. 31. This figure compiles roughness and coverage rate data of these samples for both studied rotation speeds. It appears that the film roughness continuously increases with the coverage rate of PS beads, irrespectively of the TiO_2-SiO_2 composition. It means that the final morphology is essentially controlled by the surface density of initially deposited PS beads.

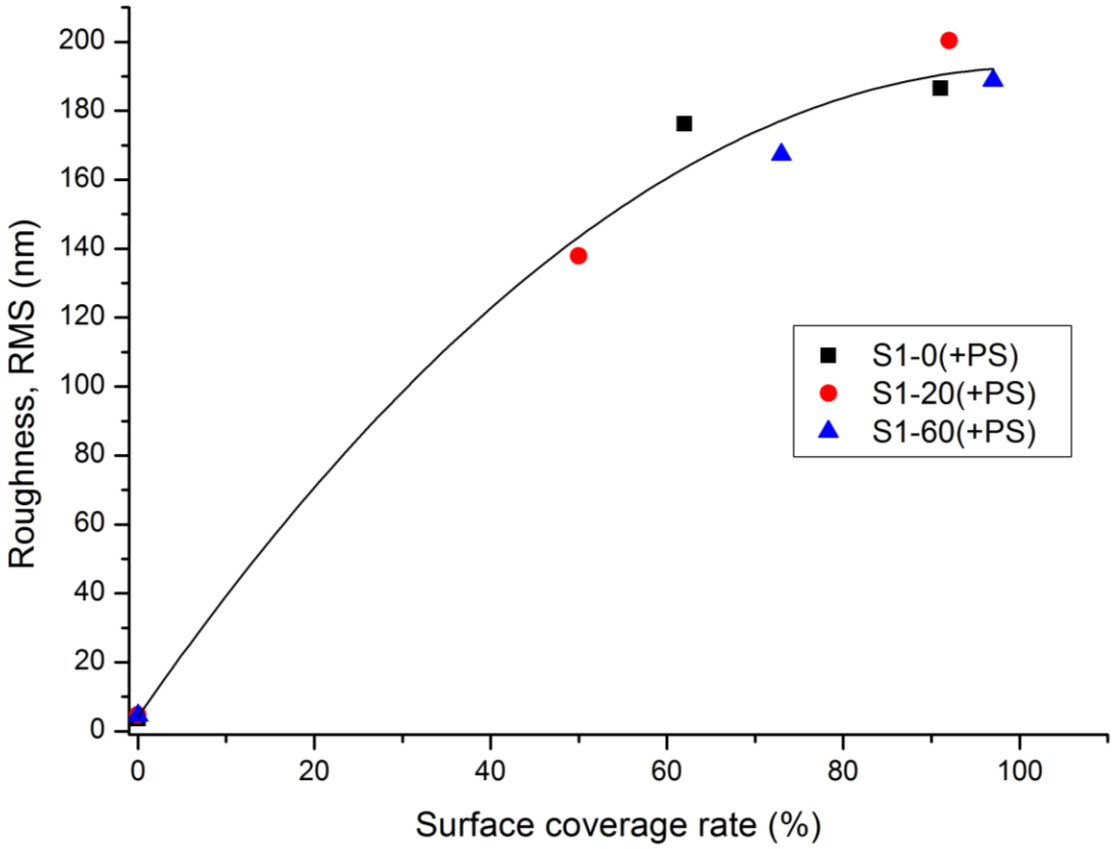

Fig. 31: Quantitative comparison of film surface roughness as a function of the surface coverage rate for S1-0(+PS) (■), S1-20(+PS) (●) and S1-60(+PS) (▲) films deposited with rotation speed 1000rpm and 500rpm. In this compilation, rotation speeds are not distinguished. The line is drawn to guide the eye

5.3.3. Rough/porous structures

Finally, FEG-SEM images are used to complete this analyze on the surface morphology of composite + PS films. These images confirm the rough structure that is obtained after post-impregnation of composite sols on a 2D layer of PS beads (see the fourth row in Fig. 27 to Fig. 30). All these observations allow concluding that, except in case of S1-100 films, the deposition of PS beads and post-impregnation of composite sols leads to films with strongly rough surface morphology compared to naturally smooth films directly deposited on silicon.

5.4. Water contact angle of composite + PS films

Water contact angles measured over 6 (experiment with 500rpm) and 11 (experiment with 1000rpm) weeks of aging on S1-X+PS composite films are summarized in Fig. 32 and compared to reference films without PS beads (data from Fig. 26).

As one can observe, compared to water contact angle measurements for reference composite films without PS, the super-hydrophilicity persistence is considerably increased in three cases: S1-0+PS, S1-20+PS and S1-60+PS. These observations are coherent with morphology features illustrated in Fig. 25 to Fig. 30, showing that the strong roughness increase induced by PS beads for S1-0+PS, S1-20+PS and S1-60+PS composite films promotes an important super-hydrophilicity enhancement. In contrast, S1-100+PS composite films do not show any improvement compared to reference S1-100 films. It even seems that the super-hydrophilicity loss is faster in the former case for the 1000rpm speed. These observations confirm that S1-100+PS films constitute a particular case that will require further studies for better understanding. Finally, it should be mentioned that, while PS beads strongly reduce the super-hydrophilicity loss of S1-0 films, aging data for S1-0+PS films are still very dispersed compared to S1-20+PS and S1-60+PS films, which is in agreement with data illustrated in Fig. 26 in the absence of PS beads.

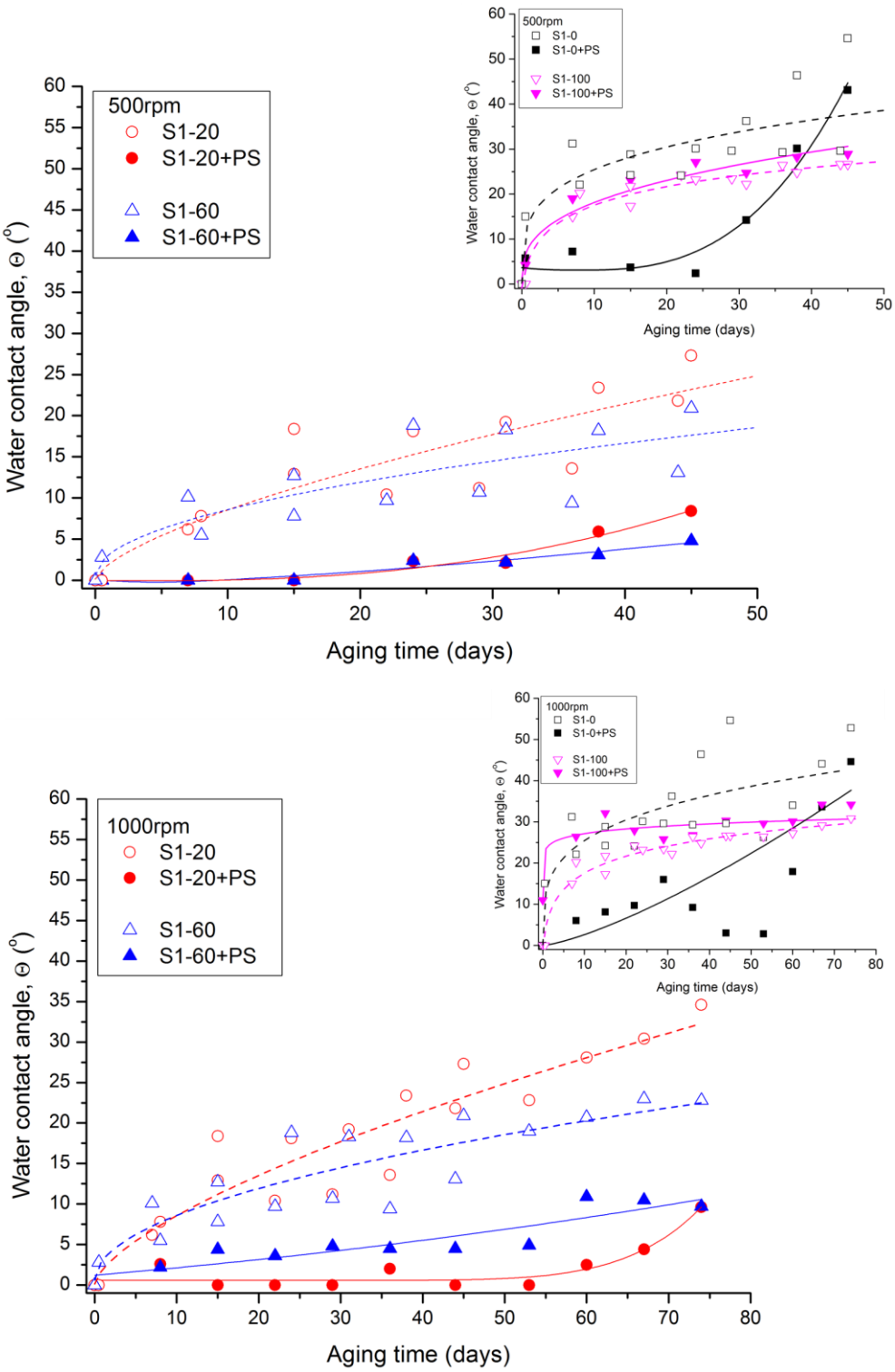

Fig. 32: Kinetics of water contact increase over aging for S1-X composite films deposited on silicon and S1-X+PS films deposited with a rotation speed of 500rpm (top) and 1000rpm (bottom). Main figures compare the kinetics measured on S1-20 films with (●) or without PS (○) and S1-60 films with (▲) or without PS (Δ). The inserts compare the same variations for S1-0 films with (■) or without PS (□) and S1-100 films with (▼) or without PS (▽)

These observations are completed in Fig. 33, which compares the water contact angle measured after 6 weeks of aging on reference composite samples and S1-X+PS samples obtained from both studied rotation speeds. This figure shows that, while roughness features enhance the super-hydrophilicity persistence of S1-0+PS, S1-20+PS and S1-60+PS samples, wettability properties are much better on both latter samples, which provides new evidence of the intrinsic effects of TiO_2-SiO_2 granular interfaces on the super-hydrophilicity of composite films. Besides, Fig. 33 suggests that the rotation speed also influences the wettability properties of these samples. As explained before, the rotation speed used for PS beads deposition controls their coverage rate, which in turn governs the final roughness of S1-X+PS composite films.

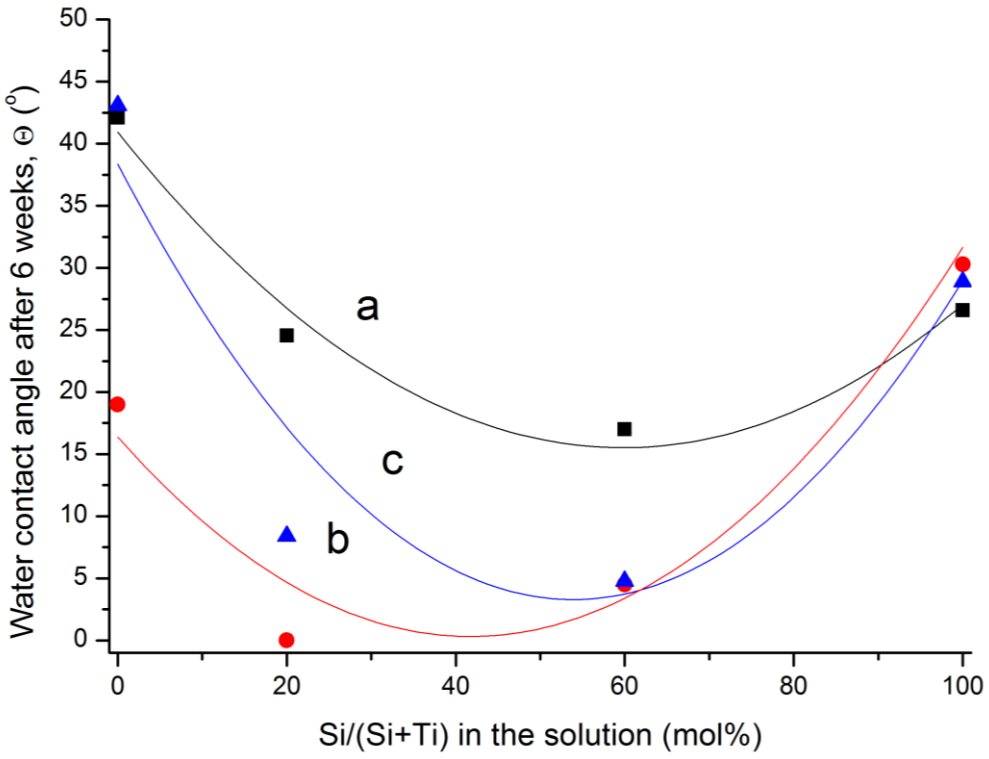

Fig. 33: Water contact angle measured after 6 weeks of aging under ambient atmosphere without UV irradiation as a function of the SiO_2 sol molar composition: reference composite samples (■, a) and composite + PS films with rotation speeds 1000rpm (●, b) and 500rpm (▲, c). Data of Fig. 33a correspond to average values derived from Fig. 26. Data of Fig. 33b have been extrapolated from fits presented in Fig. 32. The lines are drawn to guide the eye

Accordingly, we have compiled in Fig. 34 water contact angle values measured after 6 weeks of aging on S1-20 and S1-60 films formed in the absence or in the presence of PS beads deposited with both rotation speeds. In this figure, we have not presented data derived from S1-0+PS and S1-100+PS samples owing to dispersed data arising from the formers and specific features arising from the latters. It seems that, while roughness effects induced by PS beads strongly enhance the super-hydrophilicity persistence of both kinds of composite films, this influence is not necessarily confirmed when the roughness increases about a certain threshold value. It would suggest that above this threshold, roughness and composition effects are not the only ones involved in the wettability of composite films. Of course, this observation will require future experiments to draw more precise conclusions.

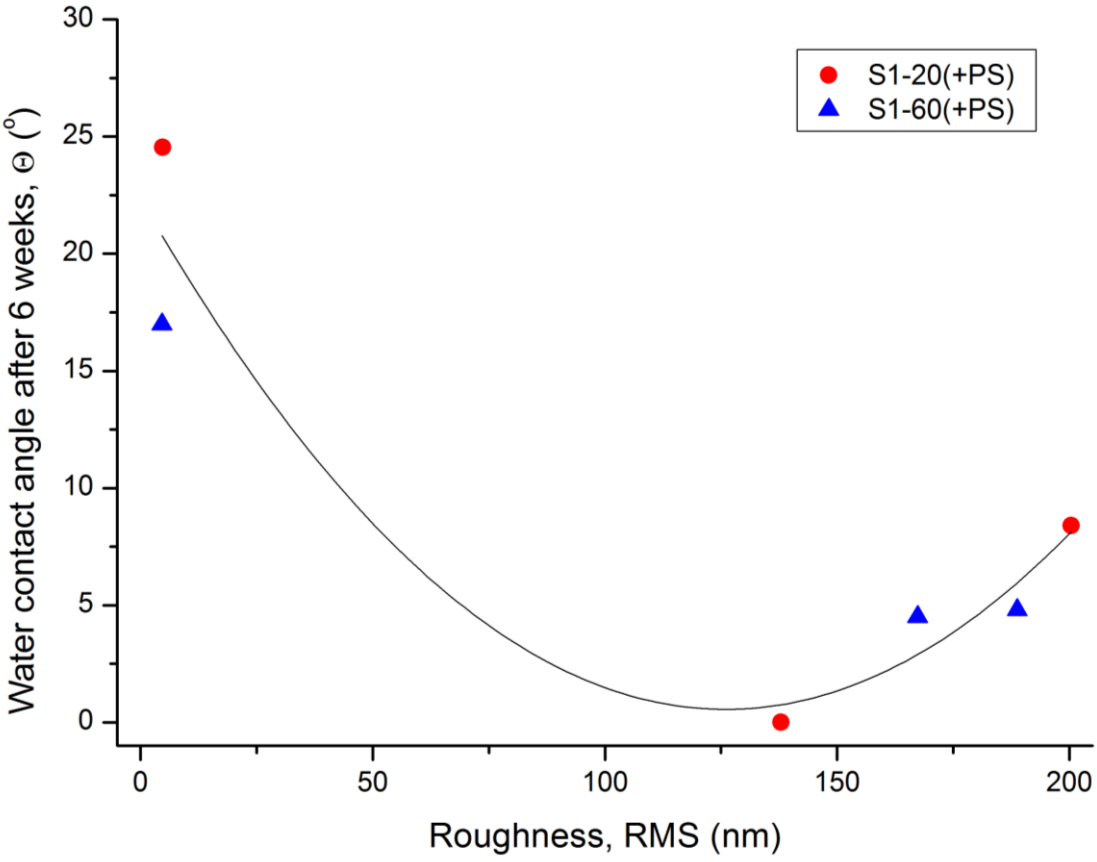

Fig. 34: Influence of the film surface roughness on the water contact angle values measured after 6 weeks of aging under ambient atmosphere without UV radiation for S1-20(+PS) (●) and S1-60(+PS) (▲) films deposited with rotation speeds 1000rpm and 500rpm (data are from Fig. 33). In this compilation, rotation speeds are not distinguished and the line is drawn to guide the eye

6. Conclusions

In this work, we have shown that it is possible to create sample surfaces with 2D layers of closely packed and well arranged PS beads of diameter *0.6μm* by spin-coating method. After calcination of PS beads, post-impregnated TiO_2-SiO_2 composite sols, which naturally yield a rather small surface roughness when deposited on Si substrate, lead to an artificially rough/porous surface morphology of S1-X+PS films with a RMS roughness value increased by about two orders of magnitude compared to similar films deposited without PS beads. Compared to reference films without PS, water contact angle measurements on composite + PS films have shown a strong increase of super-hydrophilicity persistence, especially for composite films S1-20+PS and S1-60+PS. The super-hydrophilicity of these films persists often 6 weeks of aging under ambient atmosphere without UV radiation, i.e. the water contact angle remains close to 5^o. For both films composition, this work also suggests some relation between: 1) the surface coverage of PS beads, 2) the surface roughness/porosity of S1-X+PS films, and 3) the super-hydrophilicity persistence of these films. Further studies are required to precise this relation, which introduces future perspectives to this work.

Several parameters concerning PS films elaboration, such as PS beads size, solution concentration, rotation speed and time, acceleration, deposition volume etc., that all might influence the creation of closely-packed single-layer of PS beads, must be further studied in order to vary the surface coverage, which in turn controls the values of post-impregnation RMS roughness. This effect is already observed when comparing both experiments with different rotation speeds (1000rpm and 500rpm). As well, other conditions that concern TiO_2-SiO_2 composite sols, such as solution concentration, deposition volume etc., must be tested so that the post-impregnation of composite sols would lead to surface morphologies varied in an extended range of roughness/porosity. Further studies in that sense are presently in progress.

7. References

1. Fujishima, A., Honda, K., **"Electrochemical Photolysis of Water at a Semiconductor Electrode"**, *Nature* 238 (5358) 37-38, 1972

2. Hermann, J.M., **"Heterogeneous photocatalysis : fundamentals and applications to the removal of various types of aqueous polluants"**, *Catalysis Today* 53 (1) 115-129, 1999

3. Wang, R., Hashimoto, K., Fujishima, A., Chikuni, M., Kojima, E., Kitamura, A., Shimohigoshi, M., Watanabe, T., **"Light induced amphiphilic surfaces"**, *Nature* 388 (6641) 431-443, 1997

4. Wang, R., Hashimoto, K., Fujishima, A., Chikuni, M., Kojima, E., Kitamura, A., Shimohigoshi, M., Watanabe, T., **"Photogeneration of Highly Amphiphilic TiO_2 Surfaces"**, *Advanced Materials* 10 (2) 135-138, 1998

5. Shultz, A.N., Jang, W., Hetherington, M.W., Baer, D.R., Wang, L.Q., Engelhard, M.H., **"Comparative second harmonic generation and X-ray photoelectron spectroscopy studies of the UV creation and O_2 healing of Ti^{3+} defects on (110) rutile TiO_2 surfaces"**, *Surface Science* 339 (1-2) 114-124, 1995

6. Mouboué ssi Manguendza Luce Mélissa, **"Super-hydrophilie naturelle de revêtements nano-composites TiO_2-SiO_2 déposés par voie sol-gel"**, *MSc Thesis work*, Grenoble INP, 2011

7. Yu, J.C., Yu, J., Tang, H.Y., **"Effect of surface microstructure on the photoinduced hydrophilicity of various metal oxide thin films"**, *Journal of Materials Chemistry* 12 (1) 81-85, 2002

8. Yu, J.C., Yu, J., Ho, W., Zhao, J., **"Light-induced super-hydrophilicity and photocatalytic activity of mesoporous TiO_2 thin films"**, *Journal of Photochemistry and Photobiology A Chemistry*, 148 (1-3) 331-339, 2002

9. Machida, M., Norimoto, K., Watanabe, T., Hashimoto, K., Fujishima, A.,**"The effect of SiO_2 addition in super-hydrophilic property of TiO_2 photocatalyst"**, *Journal of Materials Science* 34 (11) 2569-2574, 1999

10. Houmard, M., **"Revêtements sol-gel TiO_2-SiO_2 naturellement super-hydrophiles visant à développer des surfaces à nettoyabilité accrue"**, *PhD Thesis work*, Grenoble INP, 2009

11. Mahé, M., Vignes-Adler, M., Rouseau, A., Jacquin, C.G., Adler, P.M., **"Adhesion of droplets on a solid wall and detachment by a shear flow. I-Pure systems"**, *Journal of Colloid and Interfaces Science* 126 (1) 314-328, 1988

12. Boulangé-Petermann, L., Gabet, C., Baroux, B., **"On the respective effect of the surface energy and micro-geometry in the cleaning ability of bare and coated steels"**, *Colloids and Surfaces A: Physicochemical and Engineering Aspects* 272 (1) 56-62, 2006

13. Thoreau, V., *PhD Thesis work*, Grenoble INP, 2005

14. Thoreau, V., Malki, B., Berthomé, G., Boulangé-Petermann, L., Joud, J.C., **"Physico-chemical and dynamic study of oil-drop removal from bare and coated stainless-steel surfaces"**, *Journal of Adhesion Science and Technology* 20 (16) 1819-1831, 2006

15. Qi, L., Birnie, D.P., **"Templated titania films with meso- and microporosities"**, *Materials Letters* 61 (11-12) 2191-2194, 2007

16. Sen, T., Tiddy, G.J.T., Casci, J.L., Anderson, M.W., **"Synthesis and Characterization of Hierarchically Ordered Porous Silica Materials"**, *Chemistry of Materials* 16 (11) 2044-2054, 2004

17. Perrin, J., **"Mouvement Brownien et réalité moléculaire"**, *Annales Des Chimie Et Des Physique* 18 (1) 1-114, 1909

18. Denkov, N.D., Velev, O.D., Kralchevsky, P.A., Ivanov, I.B., Yoshimura, H., Nagayama, K., **"Mechanism of Formation of Two-Dimensional Crystals from Latex Particles on Substrates"**, *Langmuir* 8 (12) 3183-3190, 1992

19. Deckman, H.W., Dunsmuir, J.H., **"Natural Lithography"**, *Applied Physics Letters* 41 (4) 377-379, 1982

20. Colson, P., Cloots, R., Henrist, C., **"Experimental design applied to spin coating of 2D colloidal crystal masks: A relevant method?"**, *Langmuir* 27 (21) 12800-12806, 2011

21. Mihi, A., Ocaña, M., H. Míguez, H., **"Oriented colloidal-crystal thin films by spin-coating microspheres dispersed in volatile media"**, *Advanced Materials* 18 (17) 2244-2249, 2006

22. Cassie, A.B.D., Baxter, S., **"Wettability of porous structures"**, *Transactions of the Faraday Society* 40 (0) 546-551, 1944

23. Wenzel, R.N., **"Resistance of solid Surfaces to wetting by water",** *Industrial and Engineering Chemistry Research* 28 (8) 988-994, 1936

24. Bico, J., Tordeux, C., Quéré, D., **"Rough wetting"**, *Europhysics Lettres* 55 (2) 214-220, 2001

25. Langlet, M., Burgos, M., Coutier, C., Jimenez, C., Morant, C., Manson, C., **"Low Temperature Preparation of High Refractive Index and Mechanically Resistant Sol-gel TiO_2 Films for Multilayer Antireflective Coating Applications"**, *Journal of Sol-Gel Science and Technology* 22 (1-2) 139-150, 2001

26. Langlet, M., Kim, A., Audier, M., Guillard, C., Hermann, J.M., **"Liquid phase processing and thin film deposition of titania nanocrystallites for photocatalytic applications on thermally sensitive substrates"**, *Journal of Materials Science* 38 (19) 3945-3953, 2003

27. Permpoon, S., **"Revêtements TiO_2 par procédé sol-gel basse température sur acier inoxydable"**, *PhD Thesis work*, Grenoble INP, 2006

28. Primeau, N., Vautey, C., Langlet, M., **"The effect of thermal annealing on aerosol-gel deposited SiO_2 films: a FTIR deconvolution study"**, *Thin Solid Films* 310 (1-2) 47-56, 1997